Synthesis and Thermal and Hydrolytic Conversion of Heterometallic Copper Oxide–Alkoxides

John A. Samuels, Wen-C. Chiang, John C. Huffman, Kathleen L. Trojan, William E. Hatfield,* David V. Baxter,* and Kenneth G. Caulton*

Department of Chemistry, Department of Physics, and Molecular Structure Center, Indiana University, Bloomington, Indiana 47405, and Department of Chemistry, University of North Carolina, Venable and Kenan Laboratories, Chapel Hill, North Carolina 27599

Received February 25, 1994[⊗]

The synthesis, characterization, thermal decomposition, and full hydrolysis of $Cu^{I}_2Zr_2(O^iPr)_{10}$ (**1**), $Cu^{I}_4Zr_4O(O^iPr)_{18}$ (**2**), and $Cu^{II}_4Zr_4O_3(O^iPr)_{18}$ (**3**) are reported. Compound **1** is converted to compound **2** via hydrolysis. Species **1** and **2** are converted to **3** via oxidation with dioxygen. The molecular structure for **2** consists of two $[Cu_2(\mu_2\text{-}OR)_2Zr_2(\mu_2\text{-}OR)_3(OR)_4]^+$ fragments bound together via a pseudotetrahedron $\mu_4\text{-}O^{2-}$ ligand bridging the copper centers. The X-ray structure of **3** consists of a planar $Cu_4O(O^iPr)_2^{4+}$ fragment capped by two $Zr_2O(O^iPr)_8^{2-}$ face-sharing bioctahedral units. The central oxo of the copper fragment is rigorously square-planar. Magnetic studies of **3** reveal a singlet ground state both in solution and the solid state. TGA studies of **1**–**3** reveal that all the systems undergo internal redox, producing copper metal, acetone, and H_2. The final products contained an increasing amount of zirconia with increasing number of oxo ligands in the precursor species. Full hydrolysis of **1** and **3**, followed by thermolysis, produced Cu^0, Cu_2O, and CuO with zirconia depending on thermolysis conditions. Results also indicate that precursor design influences the thermolysis behavior of the solid-state product.

Introduction

Since the advent of copper-containing superconducting ceramics,[1] there has been an abundance of reports on the synthesis of copper-containing heterometallic species as potential precursors to these and other advanced materials. While these heterometallic species[2] incorporate a large range of ligand types (i.e., acetylacetonates, alkoxides (1°–3°), alkoxy ethers, alkoxyamines, oxos, diols, etc.),[3-8] little research has been undertaken to understand the specific effects these ligands have on the structural stability of the precursor and their conversion to solid-state materials. The studies that have been conducted were on homometallic systems and their thermolysis characteristics.[9]

In our continuing research on heterometallic alkoxides, we have focused on the effects of ligand composition and metal oxidation state[10] on the properties of copper-containing precursors. In the course of these investigations, we have synthesized and structurally characterized a copper–zirconium oxide–alkoxide species containing an unusual square-planar oxo ligand bridging divalent copper centers.[11] We report here the complete synthesis, characterization, and unusual structural, magnetic, and spectroscopic properties of this heterometallic oxide–alkoxide complex as well as the systematic study of the effect of oxo ligands on the stability and decomposition mechanism and products of mono- and divalent copper–zirconium isopropoxides. We also discuss attempts to produce a metastable copper–zirconium oxide via heterometallic precursors.

Experimental Section

Materials and Procedures. All manipulations were performed using standard Schlenk techniques either under a dry nitrogen atmosphere or using a nitrogen-filled drybox. Toluene, pentane, diethyl ether, and tetrahydrofuran were dried over sodium or potassium benzophenone ketyl. 2-Propanol and dichloromethane were dried over calcium hydride. All were distilled under dry nitrogen and subject to freeze–pump–thaw cycles prior to use. Dioxygen was dried over finely divided P_2O_5. $ZrCl_4(THF)_2$,[12] $Zr_2(O^iPr)_8(HO^iPr)_2$,[13] and anhydrous $CuCl_2$[14] were prepared via literature methods. $Cu^{I}_2Zr_2(O^iPr)_{10}$ was prepared via literature methods[10] with the following modifications: Toluene was used as the reaction solvent and product was recrystallized from dichloromethane giving an increased isolated yield of 45%. Potassium hydride (Aldrich) was washed repeatedly with hexanes and dried under vacuum.

Physical Measurements. ^1H and ^{13}C NMR spectra were recorded on a Nicolet NT-360 spectrometer (361 MHz and 90 MHz, respectively), a Varian 300 spectrometer (300 MHz and 75 MHz, respectively), and a Bruker AM-500 spectrometer (500 MHz and 124 MHz, respectively). Variable-temperature ^1H NMR were recorded on the Varian 300 in

* To whom correspondence should be addressed as follows: W.E.H., Department of Chemistry, University of North Carolina; D.V.B., Department of Physics, Indiana University; K.G.C., Department of Chemistry, Indiana University.

⊗ Abstract published in *Advance ACS Abstracts*, April 15, 1994.

(1) Poole, C. P. *Copper Oxide Superconductors*; Wiley, Inc.: New York, 1988.
(2) For general reviews of mixed-metal precursors, see: (a) Caulton, K. G.; Hubert-Pfalzgraf, L. G. *Chem. Rev.* **1990**, *90*, 969. (b) Chandler, C. D.; Roger, C.; Hampden-Smith, M. J. *Chem. Rev.* **1993**, *93*, 1205.
(3) (a) Bidell, W.; Shklover, V.; Berke, H. *Inorg. Chem.* **1992**, *31*, 5561. (b) Bidell, W.; Bosch, H. W.; Veghini, D.; Hund, H.-U.; Döring, J.; Berke, H. *Helv. Chim. Acta* **1993**, *76*, 596. (c) Bidell, W. Döring, J.; Bosch, H. W.; Hund, H.-U.; Plappert, E.; Berke, H. *Inorg. Chem.* **1993**, *32*, 502.
(4) (a) Purdy, A. P.; George, C. F.; Callahan, J. H. *Inorg. Chem.* **1991**, *30*, 2812. (b) Purdy, A. P.; George, C. F. *Inorg. Chem.* **1991**, *30*, 1970. (c) Coan, P. S.; Huffman, J. C.; Caulton, K. G. *Inorg. Chem.* **1992**, *31*, 4207.
(5) Sauer, N. N.; Garcia, E.; Salazar, K. V.; Ryan, R. R.; Martin, J. A. *J. Am. Chem. Soc.* **1990**, *112*, 1524.
(6) (a) Wang, S.; Trepanie, S. J.; Wagner, M. J. *Inorg. Chem.* **1993**, *32*, 833. (b) Wang, S. *Inorg. Chem.* **1991**, *30*, 2252. (c) Wang, S.; Smith, K. D. L.; Pang, Z.; Wagner, M. J. *J. Chem. Soc., Chem. Commun.* **1992**, 1594. (d) Blake, J. A.; Milne, P. E. Y.; Thornton, P.; Winpenny, R. E. P. *Angew. Chem., Int. Ed. Engl.* **1991**, *30*, 1139.
(7) Rupich, M. W.; Lagos, B.; Hachey, J. P. *Appl. Phys. Lett.* **1989**, *55*, 2447.
(8) Love, C. P.; Torardi, C. C.; Page, C. J. *Inorg. Chem.* **1992**, *31*, 1784.
(9) (a) Xue, Z.; Vaartstra, B. A.; Caulton, K. G.; Chisholm, M. H.; Jones, D. L. *Eur. J. Solid State Inorg. Chem.* **1992**, *29*, 213. (b) Whitesides, G. M.; Sudowski, J. S.; Lilburn, J. *J. Am. Chem. Soc.* **1974**, *96*, 2829. (c) Jeffries, P. M.; Dubois, L. H.; Girolami, G. S. *Chem. Mater.* **1992**, *4*, 1169. (d) Sen, A.; Rhubright, D.; Nandi, M. *Inorg. Chem.* **1990**, *29*, 3066. (e) Stecher, H. A.; Sen, A.; Rheingold, A. L. *Inorg. Chem.* **1989**, *28*, 3280.
(10) Vaartstra, B. A.; Samuels, J. A.; Barash, E. H.; Martin, J. D.; Streib, W. E.; Gasser, C.; Caulton, K. G. *J. Organomet. Chem.* **1993**, *449*, 191.
(11) Samuels, J. A.; Vaartstra, B. A.; Huffman, J. C.; Trojan, K. L.; Hatfield, W. E.; Caulton, K. G. *J. Am. Chem. Soc.* **1990**, *112*, 9623.
(12) Manzer, L. E. *Inorg. Synth.* **1982**, *21*, 136.
(13) Vaartstra, B. A.; Huffman, J. C.; Gradeff, P. S.; Hubert-Pfalzgraf, L. G.; Daran, J.-C.; Parraud, S.; Yunlu, K.; Caulton, K. G. *Inorg. Chem.* **1990**, *29*, 3126.
(14) So, J.-H.; Boudjouk, P. *Inorg. Chem.* **1990**, *29*, 1592.

0020-1669/94/1333-2167$04.50/0

benzene-d_6. Temperatures were stable to within 1 °C during the recording of each spectrum. Infrared spectra were recorded on a Nicolet 510P FT-IR as KBr pellets (s = strong, m = medium, w = weak, sh = shoulder). Thermogravimetric analysis (TGA) was carried out on a Dupont 2100 instrument installed inside a helium-filled glovebox. The TGA profile was run either under a flow of helium or dry air (1 atm, 70 cm^3/min) at a heating rate of 10 °C/min to a final temperature of 1000 °C. The effluent from the TGA sample was led into a VG micromass quadrupole mass spectrometer for identification of the volatile products. Room-temperature powder X-ray diffraction (XRD) studies were performed on a Scintag XDS 2000 powder diffractometer (Cu Kα). Variable-temperature X-ray diffraction (VT-XRD) studies were performed using a Model HT-2000C high-temperature stage, again either with a flowing He atmosphere or with the sample exposed to air. To enhance the temperature uniformity across the sample the powder was held in a small Pt boat which was placed on the Pt–Ir heating element of the stage. The temperature was recorded using a Pt–PtRh (10%) thermocouple attached to the heating element. The temperature of the powdered sample itself could differ from this reading by as much as 30 °C over the temperature range used. Scans were performed in 200 °C intervals from 500 to 900 °C. Since it was not possible to load highly air-sensitive material into the X-ray stage, scans were typically performed on material which had been previously heated in the TGA to the point where most of the organic components had been given off.

Syntheses. $K_4Zr_2O(O^iPr)_{10}$.[15] A 5.17-g sample (13.7 mmol) of $ZrCl_4(THF)_2$ was dissolved in 100 mL of THF. To this was added 50 mL of THF containing 0.12 mL (6.83 mmol) of de-ionized water. The colorless solution was allowed to stir for 30 min. In a second flask, 3.29 g (82.0 mmol) of KH was suspended in 100 mL of THF and the suspension was cooled to 0 °C. To this was added dropwise 6.51 mL (85.0 mmol) of ^{i}PrOH. When the effervescence had subsided, the reaction was allowed to warm to room temperature and stirred for an additional 30 min. The solution was then transferred via cannula to the $ZrCl_4(THF)_2/H_2O$ solution resulting in immediate formation of a colorless precipitate. After reflux for 48 h, the reaction mixture was allowed to cool and solvent was removed *in vacuo*. The resulting waxy, off-white solid was extracted with warm toluene and the solvent removed from the filtrate *in vacuo* producing a colorless, microcrystalline solid (80% yield, 95% pure by NMR). Crude product may be recrystallized from pentane giving colorless cubes. ^{1}H NMR (benzene-d_6, 24 °C, ppm): methine protons at 4.78 (sept, ^3J = 5.8 Hz, 2H), 4.66 (sept, ^3J = 6.1 Hz, 8H); methyl protons at 1.56 (d, ^3J = 5.8 Hz, 12H), 1.08 (d, ^3J = 6.1 Hz, 48H). Anal. Calcd for $C_{30}H_{70}O_{11}K_4Zr_2$: C, 38.10; H, 7.48. Found: C, 38.29; H, 7.56.

$Cu_4^IZr_4O(O^iPr)_{18}$ (2). A 1.16-g amount (1.29 mmol) of $Cu_2Zr_2(O^iPr)_{10}$ was dissolved in 30 mL of diethyl ether. To this was added dropwise 30 mL of diethyl ether containing 14 μL (0.78 mmol) of distilled water. The colorless solution was allowed to stir for 3 h. Solvent was removed *in vacuo* producing a colorless, waxy solid. Careful recrystallization from dichloromethane produced colorless, feathery solid (90% yield by NMR, 60% isolated yield). ^{1}H NMR (benzene-d_6, 25 °C, ppm): methine protons at 4.76 (sept, ^3J = 6.1 Hz, 4H), 4.62 (sept, ^3J = 6.1 Hz, 2H), 4.51 (mult, 12H); methyl protons at 1.90 (d, ^3J = 5.8 Hz, 24H), 1.48 (d, ^3J = 6.1 Hz, 12H), 1.42 (d, ^3J = 5.8 Hz, 24H), 1.38 (d, ^3J = 5.8 Hz, 24H), 1.34 (d, ^3J = 5.8 Hz, 24H). ^{13}C{^{1}H} NMR (benzene-d_6, 25 °C): Methine carbons at 71.3 (8C), 70.6 (2C), 70.5 (4C), 70.1 (4C); methyl carbons at 28.4 (8C), 27.9 (8C), 27.4 (8C), 27.2 (8C), 27.0 (4C). IR (KBr, cm^{-1}): 2965 (s), 2932 (m), 2857 (m), 2625 (w), 1462 (w), 1450 (sh), 1375 (m), 1360 (m), 1341 (w), 1190 (m), 1173 (s), 1158 (sh), 1142 (s), 1129 (s), 1020 (s), 1007 (s), 957 (s), 845 (w), 824 (m), 694 (w), 610 (m), 552 (m), 530 (sh), 494 (w), 455 (m), 436 (w). Anal. Calcd for $C_{54}H_{126}O_{19}Cu_4Zr_4$: C, 38.18; H, 7.49. Found: C, 38.05; H, 7.47. Cryoscopic solution molecular weight determination (benzene): expected, 1699; found, 1600.

$Cu_4^{II}Zr_4O_3(O^iPr)_{18}$. Method 1. A 0.28-g amount (2.11 mmol) of $CuCl_2$ was suspended in 20 mL of THF. To this was added 10 μL (0.56 mmol) of de-ionized water. The red-brown suspension was refluxed for 30 min and then allowed to cool to room temperature. In a second Schlenk flask, 1.00 g (1.06 mmol) of $K_4Zr_2O(O^iPr)_{10}$ was dissolved in 20 mL of THF. To this was added via cannula the $CuCl_2$/water suspension. The resulting blue-green solution was refluxed for 8 h. Solvent was removed *in vacuo*, and the resulting oily green solid was extracted with 40 mL of warm pentane. The volume of filtrate was reduced *in vacuo* to approximately 15 mL and layered with 20 mL of 2-propanol. After solvent diffusion, blue platelike microcrystals were isolated. The volume of the mother liquor was reduced and the flask cooled to −30 °C to produce a second crop of microcrystals (40% yield by NMR, 20% isolated yield). Microcrystals may be recrystallized from hot pentane to give high-purity X-ray-quality cobalt-blue dichroic plates.

Method 2. A 1.22-g amount (0.72 mmol) of $Cu_4Zr_4O(O^iPr)_{18}$ (**2**) was dissolved in 20 mL of toluene. The flask was then isolated from the nitrogen source and charged with 20 mL (0.82 mmol at 298 K and 1 atm) of dioxygen. The solution gradually took on a blue-green color and was allowed to stir at room temperature for 10 h. At this time, an additional 10 mL (0.41 mmol at 298K and 1 atm) of dioxygen was added and the solution allowed to stir for an additional 3 h. Solvent was then removed *in vacuo*, the resulting blue-green oily solid was dissolved in 40 mL of warm pentane and filtered, and the volume was reduced *in vacuo* to approximately 15 mL. The solution was then layered with 20 mL of 2-propanol. Final workup was identical to method 1 (50% yield by NMR, 40% isolated yield). ^{1}H NMR (benzene-d_6, 25 °C, ppm): methine peaks at 5.55 (mult, 4H), 5.42 (br, 2H), 4.55 (br, 4H), 4.37 (mult, 8H); methyl protons at 2.57 (overlapping doublets, 24H), 2.13 (d, ^3J = 5.0 Hz, 12H), 1.50 (overlapping doublets, 24H), 1.35 (overlapping doublets, 24H), 1.29 (d, ^3J = 4.5, 12H), 1.28 (d, ^3J = 5.0 Hz, 12H), 1.26–0.85 (pentane). ^{13}C{^{1}H} (toluene-d_8, 25 °C, ppm): methine carbons at 72.0 (4C), 71.3 (4C), 70.0 (4C), 66.3 (4C), 66.2 (2C); methyl carbons at 33.2 (br, 4C), 29.0 (4C), 28.4 (4C), 27.3 (mult, 20C), 26.7 (4C). IR (KBr, cm^{-1}): 2967 (s), 2932 (m), 2859 (m), 2625 (w), 1462 (w), 1450 (sh), 1375 (m), 1362 (m), 1339 (w), 1262 (w), 1175 (s), 1164 (sh), 1145 (sh), 1130 (s), 1022 (s), 1009 (s), 965 (m), 845 (w), 833 (w), 819 (sh), 803 (sh), 608 (m), 554 (m), 529 (sh), 496 (w), 488 (sh), 453 (m), 434 (w). Elemental analyses of crystalline material were invariably imperfect due to partial loss of pentane.

Hydrolysis of $Cu_2Zr_2(O^iPr)_{10}$ (1). A 1.00-g amount (1.11 mmol) of **1** was dissolved in 100 mL of THF. To this was added dropwise with stirring 100 mL THF containing 0.14 mL (7.77 mmol) of de-ionized water over a 2-h period. The resulting light amber precipitate was allowed to stir for 3 days and then filtered and dried *in vacuo* for 24 h. The resulting amber pellet was ground up under inert atmosphere producing an amber powder (**1a**). Magnetic susceptibility measurements were performed to confirm that no paramagnetic impurities (divalent copper or copper metal) were present. A portion of amber powder was exposed to air, causing a rapid color change from amber to a deep green and then eventually to turquoise blue (**1b**). The sample was exposed to air for 3 d. Anal. Found for **1a**: C, 5.89%; H, 1.59. Found for **1b**: C, 1.96; H, 1.47. This indicates some residual organic content.

Hydrolysis of $Cu_4Zr_4O_3(O^iPr)_{18}$ (3). A 0.50-g amount (0.28 mmol) of **3** was dissolved in 50 mL of THF. To this was added dropwise with stirring 50 mL of THF containing 0.055 mL (3.05 mmol) of de-ionized water over a 2-h period. The resulting turquoise blue precipitate was allowed to stir for 3 d and was then filtered and dried *in vacuo* for 24 h. The resulting green pellet was ground up and allowed to stand in air for 3 d. Anal. Found: C, 2.73; H, 1.67.

Magnetic Measurements of $Cu_4Zr_4O_3(O^iPr)_{18}$ (3). Solution (Evans Method). A 2.3 mmol solution of $Cu_4Zr_4O_3(O^iPr)_{18}$ in toluene-d_8 was

Table 1. Crystallographic Data for $Cu^{II}_4Zr_4O_3(O^iPr)_{18}$ (**3**) and $Cu^{I}_4Zr_4O(O^iPr)_{18}$ (**2**)

	2	**3**
chem formula	$Zr_4Cu_4O_{19}C_{54}H_{126}$	$Zr_4Cu_4C_{54}H_{126}O_{21}\cdot C_5H_{12}$
a, Å	18.072(5)	12.673(8)
b, Å	22.647(6)	17.482(13)
c, Å	38.309(10)	10.877(8)
α, deg		104.85(3)
β, deg	94.79(1)	113.52(3)
γ, deg		75.65(3)
V, Å^3	15 624.22	2106.85
Z	8	1
fw	1698.64	1780.26
space group	$P2_1/c$	$P\bar{1}$
T, °C	−168	−92
λ, Å	16.29	15.14
ρ_{calcd}, g cm^{-3}	0.710 69	0.710 69
μ(Mo Kα), cm^{-1}	1.444	1.371
R^a	0.0737	0.0798
R_w^b	0.0764	0.0777

^{a} $R = \sum||F_o| - |F_c||\sum|F_o|$. ^{b} $R_w = [\sum w(|F_o| - |F_c|)^2/\sum w/F_o|^2]^{1/2}$, where $w = 1/\sigma^2(|F_o|)$.

(15) Vaartstra, B. A.; Streib, W. E.; Caulton, K. G. *J. Am. Chem. Soc.* 1990, *112*, 8593.

Table 2. Selected Bond Distances (Å) and Angles (deg) for Molecules A and B of $Cu_4Zr_4O(OCH(CH_3)_2)_{18}$ (**2**)

molecule A		molecule B		molecule A		molecule B	
Zr(1)A–Zr(2)A	3.2246(20)	Zr(1)B–Zr(2)B	3.2300(20)	Zr(7)A–O(78)A	2.238(9)	Zr(7)B–O(78)B	2.194(9)
Zr(1)A–O(10)A	1.939(9)	Zr(1)B–O(10)B	1.935(10)	Zr(8)A–O(54)	1.925(10)	Zr(8)B–O(54)B	1.924(10)
Zr(1)A–O(14)A	1.942(9)	Zr(1)B–O(14)B	1.936(9)	Zr(8)A–O(58)A	1.929(10)	Zr(8)B–O(58)B	1.935(9)
Zr(1)A–O(26)A	2.163(9)	Zr(1)B–O(26)B	2.175(9)	Zr(8)A–O(62)A	2.167(8)	Zr(8)B–O(62)B	2.177(9)
Zr(1)A–O(30)A	2.101(9)	Zr(1)B–O(34)B	2.119(8)	Zr(8)A–O(66)A	2.108(9)	Zr(8)B–O(66)B	2.098(9)
Zr(1)A–O(38)A	2.203(9)	Zr(1)B–O(38)B	2.193(8)	Zr(8)A–O(74)A	2.202(8)	Zr(8)B–O(74)B	2.227(9)
Zr(1)A–O(42)A	2.232(9)	Zr(1)B–O(42)B	2.235(8)	Zr(8)A–O(78)A	2.230(9)	Zr(8)B–O(78)B	2.192(9)
Zr(2)A–O(18)A	1.921(10)	Zr(2)B–O(18)B	1.925(10)	Cu(3)A–Cu(4)A	2.6837(27)	Cu(3)B–Cu(4)B	2.6869(25)
Zr(2)A–O(22)A	1.939(9)	Zr(2)B–O(22)B	1.945(10)	Cu(3)A–O(9)A	1.821(9)	Cu(3)B–Cu(6)B	2.8894(25)
Zr(2)A–O(26)A	2.189(9)	Zr(2)B–O(26)B	2.173(9)	Cu(3)A–O(30)A	1.865(9)	Cu(3)B–O(9)B	1.810(9)
Zr(2)A–O(34)A	2.100(9)	Zr(2)B–O(30)B	2.111(8)	Cu(4)A–Cu(5)A	2.8613(25)	Cu(3)B–O(34)B	1.847(8)
Zr(2)A–O(38)A	2.193(9)	Zr(2)B–O(38)B	2.187(9)	Cu(4)A–O(9)A	1.843(9)	Cu(4)B–O(9)B	1.822(10)
Zr(2)A–O(42)A	2.226(9)	Zr(2)B–O(42)B	2.229(9)	Cu(4)A–O(34)A	1.851(9)	Cu(4)B–O(30)B	1.861(9)
Zr(7)A–Zr(8)A	3.2227(20)	Zr(7)B–Zr(8)B	3.2228(20)	Cu(5)A–Cu(6)A	2.6837(25)	Cu(5)B–Cu(6)B	2.6985(25)
Zr(7)A–O(46)A	1.942(9)	Zr(7)B–O(46)B	1.937(9)	Cu(5)A–O(9)A	1.831(9)	Cu(5)B–O(9)B	1.848(9)
Zr(7)A–O(50)A	1.921(9)	Zr(7)B–O(50)B	1.936(9)	Cu(5)A–O(70)A	1.841(8)	Cu(5)B–O(70)B	1.860(8)
Zr(7)A–O(62)A	2.188(9)	Zr(7)B–O(62)B	2.185(9)	Cu(6)A–O(9)A	1.826(9)	Cu(6)B–O(9)B	1.840(10)
Zr(7)A–O(70)A	2.111(9)	Zr(7)B–O(70)B	2.109(9)	Cu(6)A–O(66)A	1.863(9)	Cu(6)B–O(66)B	1.865(9)
Zr(7)A–O(74)A	2.222(8)	Zr(7)B–O(74)B	2.225(8)				
Zr(2)A–Zr(1)A–O(10)A	121.38(27)	Zr(2)B–Zr(1)B–O(10)B	122.4(3)	O(70)A–Zr(7)A–O(78)A	88.1(3)	O(70)B–Zr(7)–O(78)B	86.9(3)
Zr(2)A–Zr(1)A–O(14)A	122.61(27)	Zr(2)B–Zr(1)B–O(14)B	121.97(28)	O(74)A–Zr(7)A–O(78)A	69.2(3)	O(74)B–Zr(7)B–O(78)B	68.8(3)
Zr(2)A–Zr(1)A–O(26)A	42.49(23)	Zr(2)B–Zr(1)B–O(26)B	41.99(23)	Zr(7)A–Zr(8)A–O(54)A	122.8(3)	Zr(7)B–Zr(8)B–O(54)B	120.4(3)
Zr(2)A–Zr(1)A–O(30)A	115.78(26)	Zr(2)B–Zr(1)B–O(34)B	114.83(23)	Zr(7)A–Zr(8)A–O(58)A	118.9(3)	Zr(7)B–Zr(8)B–O(58)B	121.93(28)
Zr(2)A–Zr(1)A–O(38)A	42.69(23)	Zr(2)B–Zr(1)B–O(38)B	42.42(22)	Zr(7)A–Zr(8)A–O(62)A	42.51(23)	Zr(7)B–Zr(8)B–O(62)B	42.48(23)
Zr(2)A–Zr(1)A–O(42)A	43.60(23)	Zr(2)B–Zr(1)–O(42)B	43.58(22)	Zr(7)A–Zr(8)A–O(66)A	118.60(26)	Zr(7)B–Zr(8)B–O(66)B	117.68(25)
O(10)A–Zr(1)A–O(14)A	97.5(4)	O(10)B–Zr(1)B–O(14)B	98.7(4)	Zr(7)A–Zr(8)A–O(74)A	43.48(21)	Zr(7)B–Zr(8)B–O(74)B	43.60(22)
O(10)A–Zr(1)A–O(26)A	95.2(4)	O(10)B–Zr(1)B–O(26)B	99.3(4)	Zr(7)A–Zr(8)A–O(78)A	43.94(22)	Zr(7)B–Zr(8)B–O(78)B	42.75(22)
O(10)A–Zr(1)A–O(30)A	95.7(4)	O(10)B–Zr(1)B–O(34)B	98.5(4)	O(54)A–Zr(8)A–O(58)A	97.3(4)	O(54)B–Zr(8)B–O(58)B	97.0(4)
O(10)A–Zr(1)A–O(38)A	97.5(3)	O(10)B–Zr(1)B–O(38)B	163.5(4)	O(54)A–Zr(8)A–O(62)A	98.8(4)	O(54)B–Zr(8)B–O(62)B	93.6(4)
O(10)A–Zr(1)A–O(42)A	164.5(3)	O(10)B–Zr(1)B–O(42)B	95.6(4)	O(54)A–Zr(8)A–O(66)A	95.2(4)	O(54)B–Zr(8)B–O(66)B	97.8(4)
O(14)A–Zr(1)A–O(26)A	99.3(4)	O(14)B–Zr(1)B–O(26)B	97.4(4)	O(54)A–Zr(8)A–O(74)A	95.3(4)	O(54)B–Zr(8)B–O(74)B	97.3(4)
O(14)A–Zr(1)A–O(30)A	98.3(4)	O(14)B–Zr(1)B–O(34)B	94.8(4)	O(54)A–Zr(8)A–O(78)A	164.7(4)	O(54)B–Zr(8)B–O(78)B	163.0(4)
O(14)A–Zr(1)A–O(38)A	163.8(3)	O(14)B–Zr(1)B–O(38)B	96.6(3)	O(58)A–Zr(8)A–O(62)A	92.3(4)	O(58)B–Zr(8)B–O(62)B	98.2(4)
O(14)A–Zr(1)A–O(42)A	95.7(3)	O(14)B–Zr(1)B–O(42)B	164.5(3)	O(58)A–Zr(8)A–O(66)A	98.6(4)	O(58)B–Zr(8)B–O(66)B	96.8(4)
O(26)A–Zr(1)A–O(30)A	157.8(3)	O(26)B–Zr(1)B–O(34)B	156.6(3)	O(58)A–Zr(8)A–O(74)A	162.4(4)	O(58)B–Zr(8)B–O(74)B	164.2(4)
O(26)A–Zr(1)A–O(38)A	73.2(3)	O(26)B–Zr(1)B–O(38)B	72.5(3)	O(58)A–Zr(8)A–O(78)A	96.9(4)	O(58)–Zr(8)B–O(78)B	96.0(4)
O(26)A–Zr(1)A–O(42)A	74.7(3)	O(26)B–Zr(1)B–O(42)B	74.2(3)	O(62)A–Zr(8)A–O(66)A	161.0(3)	O(62)B–Zr(8)B–O(66)B	160.0(3)
O(30)A–Zr(1)A–O(38)A	86.3(3)	O(34)B–Zr(1)B–O(38)B	86.3(3)	O(62)A–Zr(8)A–O(74)A	73.6(3)	O(62)B–Zr(8)B–O(74)B	74.1(3)
O(30)A–Zr(1)A–O(42)A	90.3(3)	O(34)B–Zr(1)B–O(42)B	89.1(3)	O(62)A–Zr(8)A–O(78)A	75.1(3)	O(62)B–Zr(8)B–O(78)B	73.7(3)
O(38)A–Zr(1)A–O(42)A	68.6(3)	O(38)B–Zr(1)B–O(42)B	68.6(3)	O(66)A–Zr(8)A–O(74)A	92.4(3)	O(66)B–Zr(8)B–O(74)B	88.1(3)
Zr(1)A–Zr(2)A–O(18)A	120.0(3)	Zr(1)B–Zr(2)B–O(18)B	121.3(3)	O(66)A–Zr(8)A–O(78)A	88.2(3)	O(66)B–Zr(8)B–O(78)B	91.5(3)
Zr(1)A–Zr(2)A–O(22)A	122.62(27)	Zr(1)B–Zr(2)B–O(22)B	119.5(3)	O(74)A–Zr(8)A–O(78)A	69.6(3)	O(74)B–Zr(8)B–O(78)B	68.8(3)
Zr(1)A–Zr(2)A–O(26)A	41.87(23)	Zr(1)B–Zr(2)B–O(26)B	42.04(24)	Cu(4)A–Cu(3)A–O(9)A	43.2(3)	Cu(4)B–Cu(3)B–Cu(6)B	69.92(6)
Zr(1)A–Zr(2)A–O(34)A	116.55(25)	Zr(1)B–Zr(2)B–O(30)B	118.21(25)	Cu(4)A–Cu(3)A–O(30)A	130.2(3)	Cu(4)B–Cu(3)B–O(9)B	42.5(3)
Zr(1)A–Zr(2)–O(38)A	42.93(22)	Zr(1)B–Zr(2)B–O(38)B	42.57(22)	O(9)A–Cu(3)A–O(30)A	172.8(4)	Cu(4)B–Cu(3)B–O(34)B	131.74(28)
Zr(1)A–Zr(2)A–O(42)A	43.73(22)	Zr(1)B–Zr(2)B–O(42)B	43.72(22)	Cu(3)A–Cu(4)A–Cu(5)A	71.44(7)	Cu(6)B–Cu(3)B–O(9)B	38.0(3)
O(18)A–Zr(2)A–O(22)A	97.1(4)	O(18)B–Zr(2)B–O(22)B	98.5(4)	Cu(3)A–Cu(4)A–O(9)A	42.60(27)	Cu(6)B–Cu(3)B–O(34)B	143.3(3)
O(18)A–Zr(2)A–O(26)A	94.8(4)	O(18)B–Zr(2)B–O(26)B	98.6(4)	Cu(3)A–Cu(4)A–O(34)A	130.1(3)	O(9)B–Cu(3)B–O(34)B	173.9(4)
O(18)A–Zr(2)A–O(34)A	98.3(4)	O(18)B–Zr(2)B–O(30)B	96.4(4)	Cu(5)A–Cu(4)A–O(9)A	38.71(27)	Cu(3)B–Cu(4)B–O(9)B	42.1(3)
O(18)A–Zr(2)A–O(38)A	162.7(4)	O(18)B–Zr(2)B–O(38)B	94.2(4)	Cu(5)A–Cu(4)A–O(34)	144.4(3)	Cu(3)B–Cu(4)B–O(30)B	130.41(27)
O(18)A–Zr(2)A–O(42)A	96.4(4)	O(18)–Zr(2)B–O(42)B	162.8(4)	O(9)A–Cu(4)A–O(34)A	172.6(4)	O(9)B–Cu(4)B–O(30)B	172.0(4)
O(22)A–Zr(2)A–O(26)A	98.2(4)	O(22)B–Zr(2)B–O(26)B	92.9(4)	Cu(4)A–Cu(5)A–Cu(6)A	70.96(7)	Cu(6)B–Cu(5)B–O(9)B	42.9(3)
O(22)A–Zr(2)A–O(34)A	97.1(4)	O(22)B–Zr(2)B–O(30)B	97.9(4)	Cu(4)A–Cu(5)A–O(9)A	39.0(3)	Cu(6)B–Cu(5)B–O(70)B	131.0(3)
O(22)A–Zr(2)A–O(38)A	96.7(4)	O(22)B–Zr(2)B–O(38)B	162.0(4)	Cu(4)A–Cu(5)A–O(70)A	143.5(3)	O(9)B–Cu(5)B–O(70)B	173.1(4)
O(22)A–Zr(2)A–O(42)A	165.0(4)	O(22)B–Zr(2)B–O(42)B	97.4(4)	Cu(6)A–Cu(5)A–O(9)A	42.7(3)	Cu(3)B–Cu(6)B–Cu(5)B	71.64(7)
O(26)A–Zr(2)A–O(34)A	158.4(3)	O(26)B–Zr(2)B–O(30)B	160.0(3)	Cu(6)A–Cu(5)A–O(70)A	131.1(3)	Cu(3)B–Cu(6)B–O(9)B	37.3(3)
O(26)A–Zr(2)A–O(38)A	72.9(3)	O(26)B–Zr(2)B–O(38)B	72.7(3)	O(9)A–Cu(5)A–O(70)A	173.8(4)	Cu(3)B–Cu(6)B–O(66)B	145.0(3)
O(26)A–Zr(2)A–O(42)A	74.3(3)	O(26)B–Zr(2)B–O(42)B	74.3(3)	Cu(5)A–Cu(6)A–O(9)A	42.87(27)	Cu(5)B–Cu(6)B–O(9)B	43.1(3)
O(34)A–Zr(2)A–O(38)A	90.3(3)	O(30)B–Zr(2)B–O(38)B	93.2(3)	Cu(5)A–Cu(6)A–O(66)A	130.48(28)	Cu(5)B–Cu(6)B–O(66)B	129.84(28)
O(34)A–Zr(2)A–O(42)A	87.2(3)	O(30)B–Zr(2)B–O(42)B	87.5(3)	O(9)A–Cu(6)A–O(66)A	172.3(4)	O(9)B–Cu(6)B–O(66)B	172.6(4)
O(38)A–Zr(2)A–O(42)A	68.9(3)	O(38)B–Zr(2)B–O(42)B	68.8(3)	Cu(3)A–O(9)A–Cu(4)A	94.2(4)	Cu(3)B–O(9)B–Cu(4)B	95.4(4)
Zr(8)A–Zr(7)A–O(46)A	122.69(28)	Zr(8)B–Zr(7)B–O(46)B	123.65(26)	Cu(3)A–O(9)A–Cu(5)A	125.0(5)	Cu(3)B–O(9)B–Cu(5)B	127.0(5)
Zr(8)A–Zr(7)A–O(50)A	122.0(3)	Zr(8)B–Zr(7)B–O(50)B	120.62(27)	Cu(3)A–O(9)A–Cu(6)A	119.4(5)	Cu(3)B–O(9)B–Cu(6)B	104.7(5)
Zr(8)A–Zr(7)A–O(62)A	42.01(22)	Zr(8)B–Zr(7)–O(62)B	42.26(22)	Cu(4)A–O(9)A–Cu(5)A	102.3(4)	Cu(4)B–O(9)B–Cu(5)B	115.9(5)
Zr(8)A–Zr(7)A–O(70)A	114.31(23)	Zr(8)B–Zr(7)B–O(70)B	115.72(23)	Cu(4)A–O(9)A–Cu(6)A	122.8(5)	Cu(4)B–O(9)B–Cu(6)B	121.8(5)
Zr(8)–Zr(7)A–O(74)A	43.00(22)	Zr(8)B–Zr(7)B–O(74)B	43.64(23)	Cu(5)A–O(9)A–Cu(6)A	94.4(4)	Cu(5)B–O(9)B–Cu(6)B	94.1(4)
Zr(8)A–Zr(7)A–O(78)A	43.74(22)	Zr(8)B–Zr(7)B–O(78)B	42.69(23)	Zr(1)A–O(10)A–C(11)A	167.4(8)	Zr(1)B–O(10)B–C(11)B	165.2(12)
O(46)A–Zr(7)A–O(50)A	98.7(4)	O(46)B–Zr(7)B–O(50)B	97.3(4)	Zr(1)A–O(14)A–C(15)A	166.6(9)	Zr(1)B–O(14)B–C(15)B	171.4(8)
O(46)A–Zr(7)A–O(62)A	97.8(4)	O(46)B–Zr(7)B–O(62)B	98.8(3)	Zr(2)A–O(18)A–C(19)A	161.4(12)	Zr(2)B–O(18)B–C(19)B	171.5(9)
O(46)A–Zr(7)A–O(70)A	95.3(4)	O(46)B–Zr(7)B–O(70)B	97.7(4)	Zr(2)A–O(22)A–C(23)A	173.3(8)	Zr(2)B–O(22)B–C(23)B	162.6(14)
O(46)–Zr(7)A–O(74)A	96.7(3)	O(46)B–Zr(7)B–O(74)B	97.2(3)	Zr(1)A–O(26)A–Zr(2)A	95.6(3)	Zr(1)B–O(26)B–Zr(2)B	96.0(3)
O(46)A–Zr(7)A–O(78)A	165.3(3)	O(46)B–Zr(7)B–O(78)B	165.2(3)	Zr(1)A–O(26)A–C(27)A	137.9(7)	Zr(1)B–O(26)B–C(27)B	136.0(7)
O(50)A–Zr(7)A–O(62)A	99.4(4)	O(50)B–Zr(7)B–O(62)B	96.1(4)	Zr(2)A–O(26)A–C(27)A	122.7(7)	Zr(2)B–O(26)B–C(27)B	127.1(7)
O(50)A–Zr(7)A–O(70)A	98.3(4)	O(50)B–Zr(7)B–O(70)B	96.3(4)	Zr(1)A–O(30)A–C(31)A	127.6(9)	Zr(2)B–O(30)B–C(31)B	127.4(8)
O(50)A–Zr(7)A–O(74)A	163.5(4)	O(50)B–Zr(7)B–O(74)B	163.6(4)	Cu(3)A–O(30)A–C(31)A	119.6(9)	Cu(4)B–O(30)B–C(31)B	121.1(8)
O(50)A–Zr(7)A–O(78)A	94.9(4)	O(50)B–Zr(7)B–O(78)B	96.2(3)	Zr(2)A–O(34)A–Cu(4)A	112.7(4)	Zr(1)B–O(34)B–Cu(3)B	112.8(4)
O(62)A–Zr(7)A–O(70)A	156.1(3)	O(62)B–Zr(7)B–O(70)B	157.9(3)	Zr(2)A–O(34)A–C(35)A	126.1(8)	Zr(1)B–O(34)B–C(35)B	126.6(8)
O(62)A–Zr(7)A–O(74)A	72.8(3)	O(62)B–Zr(7)B–O(74)B	74.0(3)	Cu(4)A–O(34)A–C(35)A	121.2(8)	Cu(3)B–O(34)B–C(35)B	120.5(8)
O(62)A–Zr(7)A–O(78)A	74.5(3)	O(62)B–Zr(7)B–O(78)B	73.5(3)	Zr(1)A–O(38)A–Zr(2)A	94.4(3)	Zr(1)B–O(38)B–Zr(2)B	95.0(3)
O(70)A–Zr(7)A–O(74)A	85.9(3)	O(70)B–Zr(7)B–O(74)B	89.5(3)	Zr(1)A–O(38)A–C(39)A	123.4(8)	Zr(1)B–O(38)B–C(39)B	122.7(7)

Table 2 (Continued)

molecule A		molecule B		molecule A		molecule B	
Zr(2)A–O(38)A–C(39)A	135.1(8)	Zr(2)B–O(38)B–C(39)B	135.2(7)	Zr(8)A–O(66)A–C(67)A	127.7(8)	Zr(8)B–O(66)B–C(67)B	126.3(8)
Zr(1)A–O(42)A–Zr(2)A	92.7(3)	Zr(1)B–O(42)B–Zr(2)B	92.7(3)	Cu(6)A–O(66)A–C(67)A	121.0(8)	Cu(6)B–O(66)B–C(67)B	121.6(8)
Zr(1)A–O(42)A–C(43)A	122.9(7)	Zr(1)B–O(42)B–C(43)B	125.0(7)	Zr(7)A–O(70)A–Cu(5)A	113.9(4)	Zr(7)B–O(70)B–Cu(5)B	112.4(4)
Zr(2)A–O(42)A–C(43)A	130.0(8)	Zr(2)B–O(42)B–C(43)B	126.3(8)	Zr(7)A–O(70)A–C(71)A	125.4(7)	Zr(7)B–O(70)B–C(71)B	127.4(8)
Zr(7)A–O(46)A–C(47)A	172.3(9)	Zr(7)B–O(46)B–C(47)B	166.8(9)	Cu(5)A–O(70)A–C(71)A	120.7(7)	Cu(5)B–O(70)B–C(71)B	120.2(8)
Zr(7)A–O(50)A–C(51)A	163.8(10)	Zr(7)B–O(50)B–C(51)B	163.8(8)	Zr(7)A–O(74)A–Zr(8)A	93.5(3)	Zr(7)B–O(74)B–Zr(8)B	92.8(3)
Zr(8)A–O(54)A–C(55)A	171.2(9)	Zr(8)B–O(54)B–C(55)B	158.7(10)	Zr(7)A–O(74)A–C(75)A	122.0(8)	Zr(7)B–O(74)B–C(75)B	123.4(7)
Zr(8)A–O(58)A–C(59)A	163.8(11)	Zr(8)B–O(58)B–C(59)B	171.1(9)	Zr(8)A–O(74)A–C(75)A	134.6(8)	Zr(8)B–O(74)B–C(75)B	128.7(8)
Zr(7)A–O(62)A–Zr(8)A	95.5(3)	Zr(7)B–O(62)B–Zr(8)B	95.2(2)	Zr(7)A–O(78)A–Zr(8)A	92.3(3)	Zr(7)B–O(78)B–Zr(8)B	94.6(3)
Zr(7)A–O(62)A–C(63)A	138.4(8)	Zr(7)B–O(62)B–C(63)B	138.4(8)	Zr(7)A–O(78)A–C(79)A	125.5(7)	Zr(7)B–O(78)B–C(79)B	122.7(7)
Zr(8)A–O(62)A–C(63)A	125.9(8)	Zr(8)B–O(62B–C(63)B	124.1(8)	Zr(8)A–O(78)A–C(79)A	126.2(8)	Zr(8)B–O(78)B–C(79)B	137.1(8)
Zr(8)A–O(66)A–Cu(6)A	111.2(4)	Zr(8)B–O(66)B–Cu(6)B	112.0(4)				

prepared. Tetramethylsilane was used as the chemical shift standard. NMR spectra were recorded on a Bruker AM-500 spectrometer at 500 MHz and 21 °C. Observed contact shift = 8.3 Hz.

Solid-State Measurements. Magnetic susceptibility data were collected using a Princeton Applied Research Model 155 vibrating-sample magnetometer (VSM) equipped with a Janis Research Co. liquid-helium cryostat. The magnetometer was calibrated at 4.2 K using $HgCo(NCS)_4$.[16] The sample was sealed in a quartz sample holder. Temperatures were measured using a calibrated GaAlAs diode.

Magnetic susceptibility data were collected from 50 to 250 K in a magnetic field of 10 kOe. The data were corrected to compensate for the diamagnetism of the sample holder, the diamagnetism of the constituent atoms using Pascal's constants,[17] and the temperature-independent paramagnetism of the Cu(II) ions (60×10^{-6} emu/mol).[18] Due to the procedure used for packing and sealing the very air-sensitive compound in the sample holder, a diamagnetic correction for the sample holder could not be obtained before the magnetic measurement was taken. Therefore, the data were simulated such that a diamagnetic correction was added to the raw data. This diamagnetic correction was determined from the room-temperature moment obtained independently for this compound. The magnitude of the derived sample holder correction was in the range measured for similar sample holders. The diamagnetic correction was assumed to be constant with temperature.

The data were fit using a SIMPLEX[19] nonlinear least-squares fitting routine with the criterion of best fit being the minimum value of the function

$$F = \sum(\chi_m^{obsd} - \chi_m^{calcd})^2/(\chi_m^{obsd})^2$$

Single-Crystal X-ray Structural Determination of $Zr_4Cu_4(O)(O^iPr)_{18}$ (2). A small, well-formed crystal was cleaved from a larger sample and affixed to the end of a glass fiber using silicone grease, and the mounted sample was then transferred to the goniostat where it was cooled to −168 °C for characterization and data collection. Standard inert-atmosphere handling techniques were used throughout the investigation. A systematic search of a limited hemisphere of reciprocal space located a set of data with monoclinic symmetry and systematic absences corresponding to the unique space group $P2_1/c$. Subsequent solution and refinement of the structure confirmed this to be the proper space group. Data were collected ($6° < 2\theta < 45°$) using a standard moving crystal moving detector technique with fixed background counts at each extreme of the scan.[20] Over 22 000 unique data are available in the octant that was examined. During data collection, severe icing occurred, and during several periods, the data were unusable. In addition, several instrument malfunctions occurred. Before the data in the suspect regions could be recollected, the crystal was lost. A careful examination of the data identified those regions where the data were not reliable, and those data were removed. In all, only 19 210 data were usable, and of these, only 11 779 considered "observed" using the 2.33σ criteria. Data were corrected for Lorentz and polarization terms and equivalent data averaged. The structure was solved by direct methods (SHELXS-86) and Fourier techniques. Two independent molecules are present in the cell. Because of the questionable nature of the data, only the metal atoms were allowed to vary anisotropically. No attempt was made to include hydrogen atoms in the refinement. A final difference Fourier was essentially featureless, the largest peaks lying at the site of the metal atoms. The results of the structure determination are shown in Tables 1 and 2 and Figure 1.

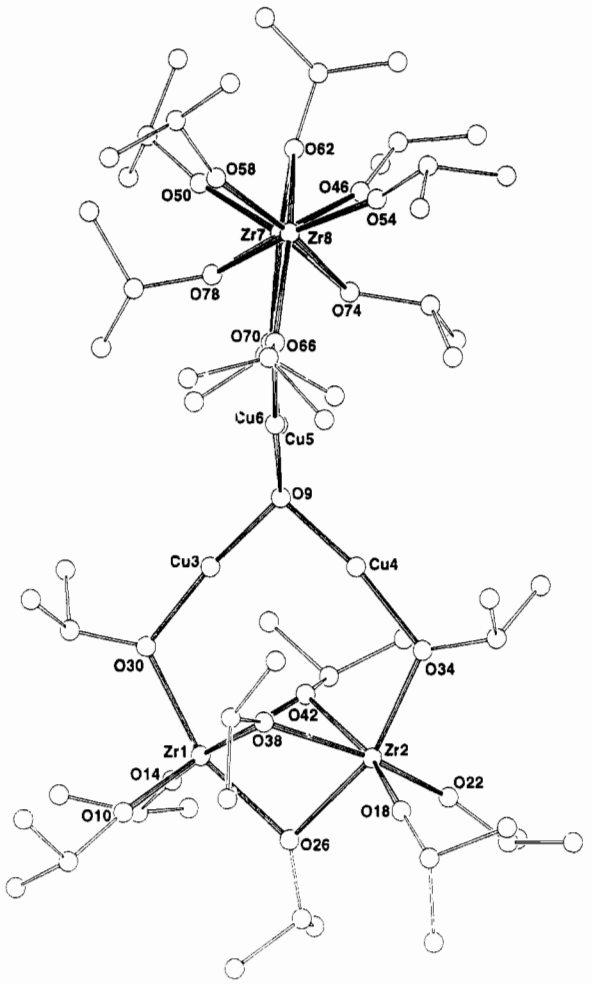

Figure 1. Ball-and-stick drawing of $Cu_4^IZr_4O(O^iPr)_{18}$ (2) showing selected atom labeling. Hydrogen atoms have been omitted for clarity.

Single-Crystal X-ray Structural Determination of $Cu_4Zr_4O_3(O^iPr)_{18}\cdot C_5H_{12}$ (3). A suitable crystal was located and transferred to thegoniostat using standard inert atmosphere handling techniques and cooled to −92 °C for characterization and data collection ($6° < 2\theta < 45°$).[20] Crystals initially cooled to −155 °C underwent a destructive phase transition. The actual temperature of the transition was not determined but appears to be near −125 °C. A systematic search of a limited hemisphere of reciprocal

(16) Brown, D. B.; Crawford, V. H.; Hall, J. W.; Hatfield, W. E. *J. Phys. Chem.* **1977**, *81*, 1303 and references therein.
(17) (a) Figgis, B. N.; Lewis, J. In *Modern Coordination Chemistry*; Lewis, J., Wilkins, R. G., Eds.; Interscience: New York, 1960; Chapter 6, p 403. (b) Kŏnig, E. *Magnetic Properties of Transition Metal Compounds*; Springer-Verlag: West Berlin, 1966. (c) Weller, R. R.; Hatfield, W. E. *J. Chem. Educ.* **1980**, *19*, 1095.
(18) Hill, N. J. *J. Chem. Soc., Faraday Trans. 2* **1976**, *72*, 631.
(19) (a) Hall, J. W. Ph.D. Dissertation, The University of North Carolina, Chapel Hill, NC, 1977. (b) Spendley, W.; Hext, G. R.; Himsworth, F. R. *Technometrics* **1962**, *4*, 441. (c) Nelder, J. A.; Mead, R. *Comput. J.* **1965**, *7*, 308. (d) O'Neill, R. *Appl. Stat.* **1971**, *20*, 338.
(20) For a general discussion of diffractometer and crystallographic procedures, see: Huffman, J. C.; Lewis, L. N.; Caulton, K. G. *Inorg. Chem.* **1980**, *19*, 2755.

Table 3. Selected Bond Distances (Å) and Angles (deg) for $Cu_4Zr_4O_3(O^iPr)_{18}$ (**3**)

Zr(1)–Zr(2)	3.205(4)	Zr(2)–O(15)	1.920(13)
Zr(1)–Cu(3)	3.915(6)	Zr(2)–O(19)	1.939(13)
Zr(1)–Cu(4)	3.126(7)	Zr(2)–O(23)	2.260(11)
Zr(2)–Cu(3)	3.111(6)	Zr(2)–O(27)	2.115(11)
Zr(2)–Cu(4)	3.868(6)	Zr(2)–O(31)	2.109(12)
Cu(3)–Cu(4)	2.781(8)	Cu(3)–O(5)	1.880(11)
Cu(3)–Cu(3)′	3.936(8)	Cu(3)–O(6)	1.9679(25)
Cu(4)–Cu(4)′	3.931(7)	Cu(3)–O(6)	1.9679(25)
Zr(1)–O(5)	2.231(11)	Cu(3)–O(31)	1.965(11)
Zr(1)–O(7)	1.939(13)	Cu(3)–O(39)	1.892(12)
Zr(1)–O(11)	1.925(13)	Cu(4)–O(5)	1.896(11)
Zr(1)–O(23)	2.124(11)	Cu(4)–O(6)	1.9655(24)
Zr(1)–O(27)	2.259(12)	Cu(4)–O(35)	1.966(11)
Zr(1)–O(35)	2.135(12)	Cu(4)–O(39)	1.901(12)
Zr(2)–O(5)	2.214(11)		

O(5)–Zr(1)–O(7)	160.1(5)	O(31)–Cu(3)–O(39)	104.0(5)
O(5)–Zr(1)–O(11)	99.6(5)	O(5)–Cu(4)–O(6)	87.4(3)
O(5)–Zr(1)–O(23)	74.3(4)	O(5)–Cu(4)–O(35)	86.0(5)
O(5)–Zr(1)–O(27)	71.7(4)	O(5)–Cu(4)–O(39)	167.0(5)
O(5)–Zr(1)–O(35)	74.2(4)	O(6)–Cu(4)–O(35)	158.8(4)
O(7)–Zr(1)–O(11)	100.1(6)	O(6)–Cu(4)–O(39)	86.8(4)
O(7)–Zr(1)–O(23)	106.1(5)	O(35)–Cu(4)–O(39)	103.4(5)
O(7)–Zr(1)–O(27)	89.3(5)	Zr(1)–O(5)–Zr(2)	92.3(4)
O(7)–Zr(1)–O(35)	99.9(5)	Zr(1)–O(5)–Cu(3)	144.3(6)
O(11)–Zr(1)–O(23)	97.1(5)	Zr(1)–O(5)–Cu(4)	98.1(5)
O(11)–Zr(1)–O(27)	167.4(5)	Zr(2)–O(5)–Cu(3)	98.6(4)
O(11)–Zr(1)–O(35)	98.2(5)	Zr(2)–O(5)–Cu(4)	140.3(6)
O(23)–Zr(1)–O(27)	72.0(4)	Cu(3)–O(5)–Cu(4)	94.9(5)
O(23)–Zr(1)–O(35)	146.9(4)	Cu(3)–O(6)–Cu(3)	179.97
O(27)–Zr(1)–O(35)	88.4(5)	Cu(3)–O(6)–Cu(4)	90.00(10)
O(5)–Zr(2)–O(15)	161.1(5)	Cu(4)–O(6)–Cu(4)	179.98
O(5)–Zr(2)–O(19)	99.0(5)	Zr(1)–O(7)–C(8)	169.2(25)
O(5)–Zr(2)–O(23)	72.1(4)	Zr(1)–O(11)–C(12)	168.8(16)
O(5)–Zr(2)–O(27)	74.8(4)	Zr(2)–O(15)–C(16)	174.5(15)
O(5)–Zr(2)–O(31)	73.5(4)	Zr(2)–O(19)–C(20)	170.9(21)
O(15)–Zr(2)–O(19)	99.4(6)	Zr(1)–O(23)–Zr(2)	93.9(4)
O(15)–Zr(2)–O(23)	90.3(5)	Zr(1)–O(23)–C(24)	139.4(10)
O(15)–Zr(2)–O(27)	106.9(5)	Zr(2)–O(23)–C(24)	126.6(10)
O(15)–Zr(2)–O(31)	100.0(5)	Zr(1)–O(27)–Zr(2)	94.2(4)
O(19)–Zr(2)–O(23)	167.0(5)	Zr(1)–O(27)–C(28)	127.4(11)
O(19)–Zr(2)–O(27)	96.7(5)	Zr(2)–O(27)–C(28)	138.3(11)
O(19)–Zr(2)–O(31)	97.7(5)	Zr(2)–O(31)–Cu(3)	99.5(5)
O(23)–Zr(2)–O(27)	72.1(5)	Zr(2)–O(31)–C(32)	135.9(11)
O(23)–Zr(2)–O(31)	88.9(4)	Cu(3)–O(31)–C(32)	121.2(11)
O(27)–Zr(2)–O(31)	146.8(4)	Zr(1)–O(35)–Cu(4)	99.2(5)
O(5)–Cu(3)–O(6)	87.7(3)	Zr(1)–O(35)–C(36)	133.5(13)
O(5)–Cu(3)–O(31)	84.5(5)	Cu(4)–O(35)–C(36)	123.3(12)
O(5)–Cu(3)–O(39)	169.4(5)	Cu(3)–O(39)–Cu(4)	94.3(5)
O(6)–Cu(3)–O(31)	155.2(3)	Cu(3)–O(39)–C(40)	121.3(13)
O(6)–Cu(3)–O(39)	87.0(4)	Cu(4)–O(39)–C(40)	114.4(13)

space located a set of diffraction maxima with no symmetry or systematic absences corresponding to one of the triclinic space groups. Subsequent solution and refinement of the structure confirmed the centrosymmetric choice. Data were collected in the usual manner using a continuous θ–2θ scan with fixed backgrounds. Data were reduced to a unique set of intensities and associated σ's in the usual manner. The structure was solved by a combination of direct methods (MULTAN78) and Fourier techniques. A difference Fourier synthesis revealed the location of some, but not all, hydrogen atoms. All hydrogen atom positions were therefore calculated using idealized geometries and d(C–H) = 0.95 Å. These calculated positions were fixed for the final cycles of the refinement. The molecule lies at a crystallographic center of inversion, with O(6) lying at the origin. There is also a disordered pentane molecule lying at a center of inversion in the lattice. A final difference Fourier was featureless, with the largest peak being 1.04e/Å^3. No absorption correction was performed. Results of the structural determination are shown in Tables 1 and 3 and Figures 2 and 3.

Results

Reactions of $Cu_2^IZr_2(O^iPr)_{10}$ with Dry O_2. The previously reported heterometallic alkoxide species $Cu_2^IZr_2(O^iPr)_{10}$ (**1**) is very air-sensitive.[10] In order to further investigate this phenomenon, reactions between **1** and dry oxygen in C_6D_6 were conducted in resealable NMR tubes and monitored by proton NMR.

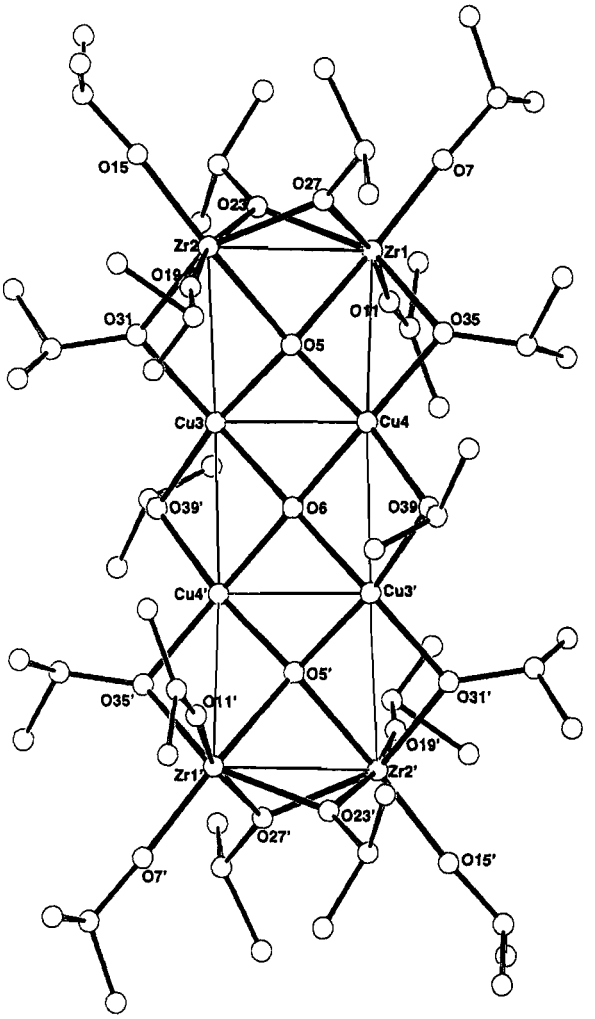

Figure 2. Ball-and-stick drawing of $Cu_4^{II}Zr_4O_3(O^iPr)_{18}$ (**3**) showing selected atom labeling. Hydrogen atoms have been omitted for clarity. The view is perpendicular to the copper–oxygen plane.

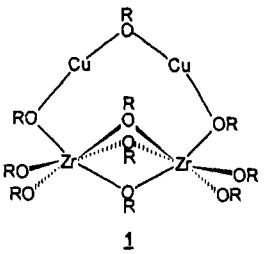

1

Initial reactions were conducted with a <1/2:1 O_2 to **1** mole ratio. At room temperature, the reaction required less than 1 h to go to completion with the colorless solution rapidly turning to a blue-green. ^{1}H NMR spectra of the sample indicated approximately 60% consumption of **1** and new signals corresponding to $Cu_4^{II}Zr_4O_3(O^iPr)_{18}$ (**3**) and acetone, plus a broad signal at 1.05 ppm. Addition of another 0.5 mol of O_2 converted the remaining monovalent copper species to **3** and additional acetone and increased the intensity of the broad signal at 1.05 ppm. The reaction rate was now retarded, requiring several hours to go to completion. This we attribute to the presence of free alcohol (see below). Upon complete consumption of **1**, reaction volatiles were vacuum transferred to a second NMR tube and the colorless solution was analyzed via ^{1}H NMR. The only species detected were acetone and 2-propanol in a 1:1 mole ratio. The blue-green reaction residue was redissolved in C_6D_6. ^{1}H NMR spectra

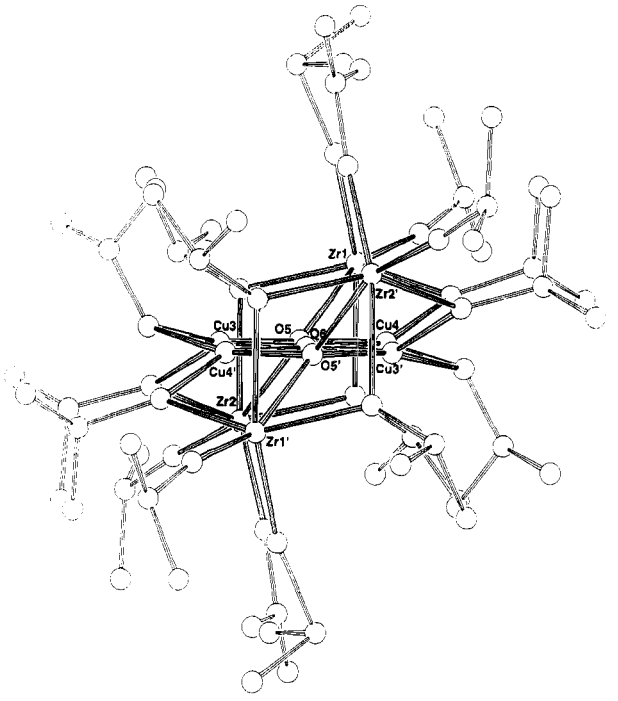

Figure 3. Ball-and-stick drawing of $Cu_4^{II}Zr_4O_3(O^iPr)_{18}$ (**3**) viewed down the vector defined by the three oxo ligands. Note the dihedral angle between the copper and zirconium planes and the distinct geometry at O(5) and O(6).

indicated only signals for **3** and a very broad feature at 1.1 ppm (~100 Hz at half-height).[21] Over the course of the entire reaction, no other signals were observed in the range of +100 to −100 ppm. On the basis of these ^{1}H NMR results, eq 1 describes the oxidation.

$$2Cu_2^{I}Zr_2(O^iPr)_{10} + {}^3/_2O_2 \rightarrow Cu_4^{II}Zr_4O_3(O^iPr)_{18} + HO^iPr + OCMe_2 \quad (1)$$

The proton NMR spectrum of **1** in the presence of excess alcohol (>5 equiv in C_6D_6) shows loss of the signals corresponding to the $Cu_2(\mu_2\text{-}O^iPr)$ group and the broadening of the free alcohol peak. None of the other signals for **1** are affected. This indicates that selective exchange occurs for this alkoxide ligand with free alcohol.[10] Oxidation of **1** in the presence of free alcohol results in a greatly retarded reaction rate, the rate being comparable to that observed in the oxidation of **2** (see below). This slowing of the oxidation rate of **1** in the presence of free alcohol is attributed to the formation of an alcohol adduct. Such a species is likely to have greater steric bulk, thereby shielding the copper centers from O_2 attack. The presence of an added ROH in **1**·ROH will

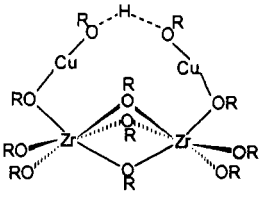

1·ROH

also make copper less electrophilic. This alcohol adduct should also result in increased electron density at copper, making the metal less likely to coordinate O_2. The ^{1}H NMR of **1** in the presence of 30 equiv of 2-propanol-d_8 in benzene-d_6 results in loss of the signal for the $Cu_2(\mu_2\text{-}O^iPr)$ group in time of mixing. The remainder of the alkoxides undergo much slower exchange with the deuterated alcohol, requiring 1 h to reach equilibrium. All these latter signals show a similar rate of decay. This indicates that either all the alkoxides undergo exchange with free alcohol at the same rate or, more likely, that all the alkoxides are undergoing intramolecular migrations at a rate faster than alcohol exchange.

Reaction of $Cu_2^{I}Zr_2(O^iPr)_{10}$ with Water. We have thus established that, in $Cu_2^{I}Zr_2(O^iPr)_{10}$, the alkoxide ligand bridging the two monovalent copper centers preferentially exchanges with free alcohol present in solution. Given the apparent strong Brønsted basicity of this alkoxide oxygen, it was thought that hydrolysis could be effected selectively at this position. This was, in fact, achieved by the reaction of 2 equiv of **1** with 1 equiv of water in diethyl ether. The colorless solution was allowed to stir for several hours at room temperature producing no change in physical appearance. The solvent was removed *in vacuo*. The ^{1}H NMR spectrum of the resulting colorless, waxy solid revealed that the reaction had produced only one major product (~95% pure). The methyl region contained five new doublets of intensity 12:6:12:12:12, while the methine region contained numerous overlapping septets between 4.9 and 4.4 ppm (with total intensity 9). Absent were the upfield signals corresponding to the $Cu_2(\mu_2\text{-}O^iPr)$ group found in **1**. This seemed to indicate that the alkoxide bridging the copper atoms had been substituted by either an oxo or hydroxo ligand resulting in a molecular formula of either $Cu_4^{I}Zr_4O(O^iPr)_{18}$ or $Cu_2^{I}Zr_2(OH)(O^iPr)_9$, respectively. IR spectra revealed no O–H stretch thus lending support to the presence of an oxo ligand. Finally, cryoscopic molecular weight studies of this compound indicated a molecular weight of 1600, which rules out $Cu_2Zr_2(OH)(O^iPr)_9$ (MW = 857). On the basis of reaction stoichiometry, spectroscopic evidence, solution molecular weight, and structure precedent, structure **2** was proposed, but the geometry around the central oxo group remained unknown. This structure has five different methyl group environments, which is in agreement with NMR results.

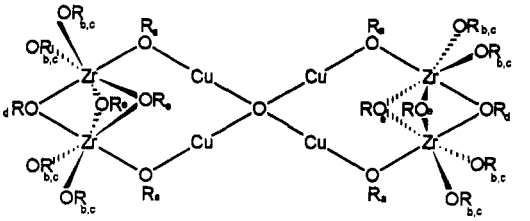

2

Pure **2** can be obtained from cold dichloromethane as a colorless, feathery solid in 60% yield. Species **2** is highly air- and oxygen-sensitive. The molecule undergoes exchange with 2-propanol (approximately 30 equiv in C_6D_6) at a rate comparable to that of **1**. This indicates the presence of the $Cu_2(O^iPr)$ group in **1** has little effect on the overall alcohol exchange process. Complex **2** was found to be unstable in pure 2-propanol-d_8, behaving similar to **1** (see above). To determine the geometry of the central oxo ligand, a single-crystal X-ray study was performed.

Solid-State Structure. A sample of **2** was crystallized from dichloromethane via slow evaporation as colorless plates with the empirical formula $Cu_4Zr_4O(O^iPr)_{18}$. The unit cell contains two crystallographically-independent molecules, so all bond lengths have been multiply-determined. The molecule (Figure 1) consists of two $Cu_2Zr_2(O^iPr)_9^+$ fragments linked through the four copper centers via a pseudotetrahedral O^{2-} ligand. This results in an idealized D_{2d} symmetry for the molecule, consistent with NMR results. The two planes defined by the four metals of each fragment are approximately perpendicular (dihedral angle = 74.0° for molecule A and 73.3° for molecule B). The $Cu_2Zr_2(O^iPr)_9^+$ fragments are nearly isostructural with **1**,[10] consisting of a $Zr_2(OR)_9$ face-shared bioctahedron bound to the two copper centers

(21) This latter species was not isolated, and no further characterization was performed. Integration (benzene standard) showed a 1:2 ratio of **3** to the 1.1 ppm species.

via two μ_2-alkoxides. In the case of **2**, the coppers are bridged by an oxo ligand giving the metal centers a two-coordinate linear geometry (172.9° average). The copper–oxo distances (average value 1.827(12) Å) are not significantly shorter than the $Cu_2(\mu_2$-$O^iPr)$ distances in **1**.

The central oxygen is distorted from idealized tetrahedral geometry in two ways. The first is the pinching of the Cu(3)–O(9)–Cu(4) and the Cu(5)–O(9)–Cu(6) angles to 94.2(4) and 94.4(4)° average (from 109.5°). This results in an increase of all other Cu–O(9)–Cu angles. The second is the bending of molecule at the central oxo. This is evident in that the two idealized C_2 axes of each Cu_2Zr_2O fragments are not precisely colinear. The angles in the two independent molecules are 6.9° in molecule A and 9.2° in molecule B. This is likely the result of crystal packing forces and the plasticity of a single oxo bridge.

Reactions of 2 with Oxygen. Investigation of the reactions between **2** and O_2 were conducted in an NMR tube analogous to our study of **1**. The initial O_2:**2** stoichiometry was 0.5:1. Upon introduction of oxygen, the colorless reaction mixture changed color to a medium forest green over a period of 2 h. ^1H NMR spectra indicated the slow decay of signals corresponding to **2** and the appearance of signals corresponding to **3** ($Cu^{II}_4Zr_4O_3(O^i$-$Pr)_{18}$) and acetone, plus a broad signal at 1.05 ppm. The reaction required at least 12 h to consume 60% of **2**, and an addition of a second 0.5 equiv of O_2 resulted in complete consumption of **2** and an increase in the intensity of the product signals. Although the sample was scanned from +100 to -100 ppm, no other signals were observed. Upon completion of the reaction, volatiles were vacuum transferred and analyzed by ^1H NMR. The colorless solution was found to contain a 1:1 ratio of acetone to 2-propanol, identical to the ratio found for the reaction of **1** with O_2. Given the anticipated reaction stoichiometry (eq 2), acetone and

$$\underset{\mathbf{2}}{Cu_4{}^{I}Zr_4O(O^iPr)_{18}} + O_2 \rightarrow \underset{\mathbf{3}}{Cu_4{}^{II}Zr_4O_3(O^iPr)_{18}} \quad (2)$$

2-propanol are apparently the products of a side reaction. The dark blue-green residue of the reaction was then redissolved in C_6D_6, and the solution was analyzed by ^1H NMR. The spectrum indicated signals for **3** and a very broad feature at 1.1 ppm (~100 Hz at half-height). The integration of the signals corresponding to **3** to the signal at 1.05 is approximately 1:1, indicating a 50% yield of the desired product. These results are very similar to those observed for the reaction of **1** with O_2. No other signals were observed in the range of +100 to -100 ppm.

Bulk Synthesis of $Cu_4^{II}Zr_4O_3(O^iPr)_{18}$ (3) from 2. The large-scale reaction of excess oxygen with **2** (>1:1 mole ratio) in toluene required extended reaction times compared with those observed in the NMR tube experiments; over 3 h are required for significant amounts of color to appear. After 10 h, additional oxygen was introduced to the deep blue-green solution to ensure complete conversion. The ^1H NMR spectrum of the reaction mixture indicates approximately 50% conversion to the desired species (**3**). A more precise estimate is difficult due to the paramagnetic nature of the byproducts. Removal of the solvent and extraction of the oily blue-green solid with pentane yields a deep blue-green solution. Careful reduction of volume and layering with 2-propanol produces blue-green platelike microcrystals of **3** in 35–40% yield.

Synthesis of $Cu_4^{II}Zr_4O_3(O^iPr)_{18}$ from $K_4Zr_2O(O^iPr)_{10}$ and $CuCl_2$. The combination salt metathesis/hydrolysis reaction (eq 3) was carried out in tetrahydrofuran. Although addition of the

$$2K_4Zr_2O(O^iPr)_{10} + 4CuCl_2 + H_2O \xrightarrow[\Delta]{THF} \underset{\mathbf{3}}{Cu_4{}^{II}Zr_4O_3(O^iPr)_{18}} + 8KCl + 2HO^iPr \quad (3)$$

$CuCl_2/H_2O$ suspension to the solution of $K_4Zr_2O(O^iPr)_{10}$ results in an immediate formation of a blue-green color, periodic analysis by ^1H NMR indicates that reflux temperatures are required to drive the reaction to completion. It should be noted that extended reflux time (>8 h) actually causes some decomposition of the desired product. After removal of the solvent *in vacuo* and extraction of the blue-green solid with pentane, the resulting clear, blue-green solution was found to contain approximately 40% **3**. Other products were uncharacterized. Workup as in the previous section produces blue-green platelike microcrystals of **3** in 20–25% yield.

Recrystallization of **3** from warm pentane results in large cobalt blue dichroic (emerald green) plates. One equivalent of pentane is found trapped in the crystalline lattice. While this pentane is not readily removed in vacuum, it does slowly diffuse out of the crystalline solid after prolonged (weeks) storage under inert atmosphere.

Compound **3** is moderately soluble in nonpolar solvents and poorly soluble in polar solvents. The species is water-sensitive both in solution and the solid state, forming a turquoise solid, but is found (by NMR) to be inert to dry oxygen. The alkoxide ligands of **3** show no line broadening or coalescence with free 2-propanol, even at 80 °C on the NMR time scale, but alcohol exchange is complete with deuterated 2-propanol (100 equiv in benzene-d_6) in less than 5 min.

Solid-State Structure. A sample of **3** was crystallized from warm pentane as cobalt-blue dichroic plates with the empirical formula $Cu_4Zr_4O_3(O^iPr)_{18}\cdot C_5H_{12}$. The molecule (Figure 2 and 3) is found to be centrosymmetric, containing a crystallographic inversion center lying at the central oxo (O(6)) and has idealized C_{2h} symmetry. The structure may be visualized as having a planar $Cu_4O(O^iPr)_2^{4+}$ fragment capped by two $Zr_2O(O^iPr)_8^{2-}$ face-sharing bioctahedral units with the four zirconium centers being coplanar. The resulting intersecting planes have a dihedral angle of 52.4(3)°. The zirconia and copper structural moieties are bound together via two μ_4-distorted tetrahedral oxo ligands (O(5)) and four μ_2-alkoxide oxygens (O(31), O(35)).

The copper coordination environment is essentially square-planar, each surrounded by two alkoxides and two oxo ligands with distances ranging from 1.880(1) to 1.968(3) Å. This configuration produces Cu–Cu distances of 2.781(8) Å, a value found to be just under the combined van der Waals radii (2.80 Å).[22] The zirconium atoms have distorted octahedral environments with each metal surrounded by five alkoxides and one oxo ligand. Zirconium–oxygen bond distances are in the following order: terminal alkoxides (1.931Å average) < Zr–O(Cu)(μ_2-alkoxides) (2.122 Å average) < Zr–O(Zr)(μ_2-alkoxides) (2.190 Å average) < Zr–O(Zr)(μ_4-oxo) (2.223 Å average). It is interesting to note that the $Zr_2(\mu$-$O^iPr)$ bridging alkoxides are bound asymmetrically, with each metal having a long and a short ligand bond (2.260 vs 2.120 Å). This phenomenon is due to steric interactions between the zirconium bridging alkoxides and the ligands of the copper portion of the molecule. The long Zr–(μ_2-OR) bond is found to be the one perpendicular to the Cu_4O plane (see Figure 3) and experiences the most ligand–ligand repulsion with the central part of the molecule. To minimize these interactions, the bond lengthens, moving the bulky alkoxide group away from the Cu_4O plane.

Terminal alkoxides bound to zirconium in **3** are found to be nearly linear ($\angle$Zr–O–C ≥ 168.8(16)°) and bridging alkoxides bound to zirconium are approximately planar (angles sum to >356.0°). This is consistent with π donation from the alkoxide oxygen lone pair to the empty d orbitals of the metal. In contrast, the alkoxide ligands bound solely to copper (O(39)) are pyramidal in geometry (angles sum to 330.0°). This would indicate the presence of a stereochemically-active lone pair on the oxygen and a lack of significant π donation to the d^9 metal centers. It is interesting to note that the angle sum about O(39) in **3** and the

(22) Bondi, A. *J. Phys. Chem.* **1964**, *68*, 441.

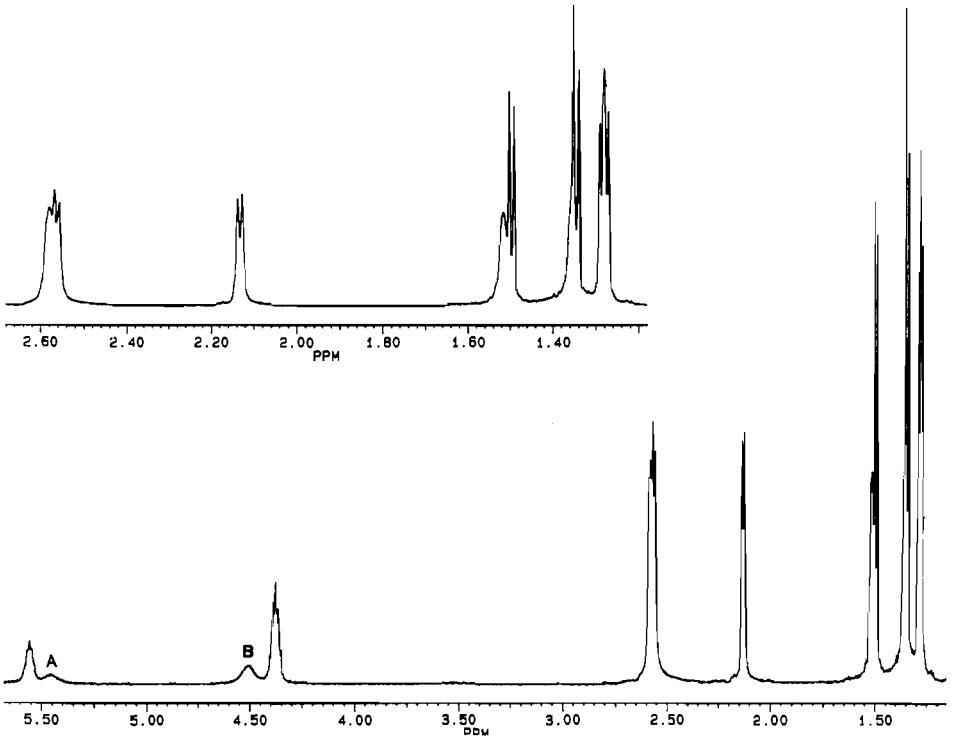

Figure 4. Proton NMR spectrum of 3 in C_6D_6 at 500 MHz. Signals A and B are assigned to the methine protons of the $Cu_2^{II}(\mu_2\text{-}O^iPr)$ and $Cu^{II}Zr(\mu\text{-}O^iPr)$ groups, respectively. Insert: Expansion of methyl region.

copper-bridging alkoxide oxygen in **1** are nearly identical (332.8° for the latter)[10] even though the oxidation states of the copper differ.

Two geometries are found for the oxo ligands in **3**. The first is an unusual[23] μ_4-square-planar oxo ligand (O(6)) bridging four copper centers. This ligand is rigorously planar with all Cu–O(6) bonds identical to within 1σ (1.966(25) Å average) and all Cu–O–Cu angles 90.00(10)°. The second geometry is pseudotetrahedral (O(5)) with each oxo bridging two copper and two zirconium centers. The distortion from true tetrahedral geometry (dihedral angle at O(5) = 52.3 *vs* 90° at a T_d center) is apparently due to the geometric constraints of the heterometallic bridging alkoxide. An alternative view is that O(5) is distorted from the planarity found in O(6) due to the different electronic effects of the d^0 zirconium ion *vs* the d^9 copper ion. This may be due to the electronic effects of the unpaired electrons or the preference of Zr for an octahedral geometry (see Discussion).

The best overall structural view of **3** is as a fragment of inorganic copper–zirconium oxide encapsulated by an organic alkoxide shell.

Spectroscopic Analysis. Spectroscopic results for **3** are in agreement with the solid-state structure. IR spectra lack any O–H stretches, thus excluding the presence of hydroxyls or coordinated alcohol. NMR spectra (^1H and ^{13}C) at 25 °C lack much of the shifting and broadening expected for paramagnetic species (Figure 4). The ^1H NMR spectrum at 25 °C shows, for the methyl region, nine doublets of 12 protons each. The large number of environments is due to the diastereotopic nature of the isopropoxide groups. The number of signals indicates that the solid-state structure is maintained in solution. In the methine region, four multiplets are observed at 5.55 (4H), 5.42 (2H), 4.55 (4H), and 4.37 (8H) ppm. The $^{13}C\{^1H\}$ NMR is also in agreement with the solid-state structure.

Variable-temperature ^1H NMR (25–80 °C) studies in C_6D_6 reveal the paramagnetic nature of **3** and allow assignment of some of the alkoxide signals. Upon heating, signals A and B (Figure 4) shift downfield at a rate of 0.05 and 0.03 ppm/°C,

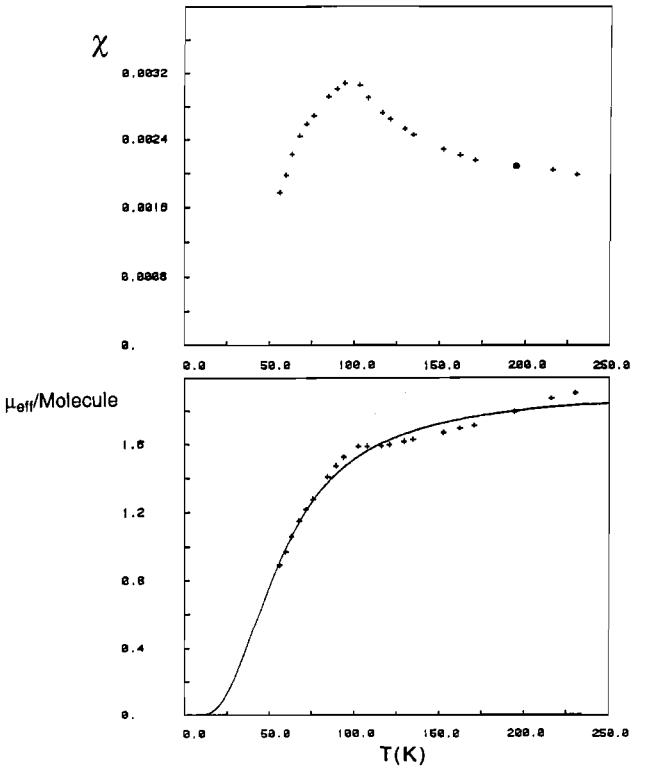

Figure 5. Solid-state magnetic susceptibility and μ_{eff} of 3. The solid line shows μ_{eff} calculated with parameters given in the text.

respectively. The other methine signals (5.55 and 4.37 ppm) are relatively unaffected, appearing to only broaden with increasing temperature. Given the dramatic effect temperature has on signals A and B, in conjunction with their absolute intensity (2:4), signal A was assigned to the alkoxide bridging the two copper centers and signal B assigned to the isopropoxides bridging copper to zirconium. In the methyl region, the corresponding signals broaden with increasing temperature. The overlapping doublets

(23) (a) Rambo, J. A.; Huffman, J. C.; Christou, G.; Eisenstein, O. *J. Am. Chem. Soc.* **1989**, *111*, 8027. (b) Cotton, F. A.; Shang, M. *J. Am. Chem. Soc.* **1990**, *112*, 1584.

become more resolved as three sets of doublets[24] (2.57, 1.50, and 1.35 ppm; intensity 12:12:12) shift downfield. By 80 °C, the methyl resonances had broadened into three nondescript features at 2.75, 2.15, and 1.40 ppm. While much of the broadening of the proton signals at high temperatures is due to paramagnetic effects, the possibility of some intramolecular alkoxide migration cannot be excluded.

Magnetism. Given the weak paramagnetic influence on the NMR spectra of **3**, magnetic characterization was undertaken for both the solid state and solution.

(a) Solid State. The magnetic susceptibility of a powdered sample of **3** is given as function of temperature in Figure 5, where it may be seen that the susceptibility exhibits a maximum value at approximately 100 K. The Heisenberg spin–spin exchange Hamiltonian

$$\mathcal{H} = -2\sum_{i<j} J_{ij}\hat{S}_i\hat{S}_j$$

was used to describe the magnetic interactions, where J_{ij} is the exchange constant and i and j number the magnetic ions. For the interaction of four copper ions, the complete Hamiltonian is

$$\mathcal{H} = -2(J_{12}\hat{S}_1\cdot\hat{S}_2 + J_{13}\hat{S}_1\cdot\hat{S}_3 + J_{14}\hat{S}_1\cdot\hat{S}_4 + J_{23}\hat{S}_2\cdot\hat{S}_3 + J_{24}\hat{S}_2\cdot\hat{S}_4 + J_{34}\hat{S}_3\cdot\hat{S}_4)$$

For a centrosymmetric four-copper array labeled as

Cu1 Cu2

Cu4 Cu3

the Hamiltonian can be reduced to

$$\mathcal{H} = -2(2J_{12}\hat{S}_1\cdot\hat{S}_2 + 2J_{13}\hat{S}_1\cdot\hat{S}_3 + 2J_{14}\hat{S}_1\cdot\hat{S}_4)$$

Solving the 16 × 16 energy matrix yields one quintet ($S' = 2$), two singlets ($S' = 0$), and three triplets ($S' = 1$). The expression for the energy levels of the states are

$$E_Q = -{}^1/_2(2J_{12} + 2J_{13} + 2J_{14})$$

$$E_{T_1} = -{}^1/_2(2J_{12} - 2J_{13} - 2J_{14})$$

$$E_{T_2} = {}^1/_2(2J_{12} + 2J_{13} - 2J_{14})$$

$$E_{T_3} = {}^1/_2(2J_{12} - 2J_{13} + 2J_{14})$$

$$E_{S_1} = {}^1/_2[2J_{12} + 2J_{13} + 2J_{14} + 2\sqrt{(2J_{12} - J_{13} - J_{14})^2 + 3(J_{13} - J_{14})^2}]$$

$$E_{S_2} = {}^1/_2[2J_{12} + 2J_{13} + 2J_{14} - 2\sqrt{(2J_{12} - J_{13} - J_{14})^2 + 3(J_{13} - J_{14})^2}]$$

The following resulting expression was used to fit the observed magnetic susceptibility:

$$\chi_m = \frac{N_g{}^2\beta^2}{3kT}\sum_{S'}\frac{S'(S'+1)(2S'+1)\exp(-E_i/kT)}{(2S'+1)\exp(-E_i/kT)}$$

(24) Since the copper-bridging alkoxide lies on a mirror plane, its methyl groups are not diastereotopic. Therefore, three sets of methyl signals correspond to two sets of methine signals.

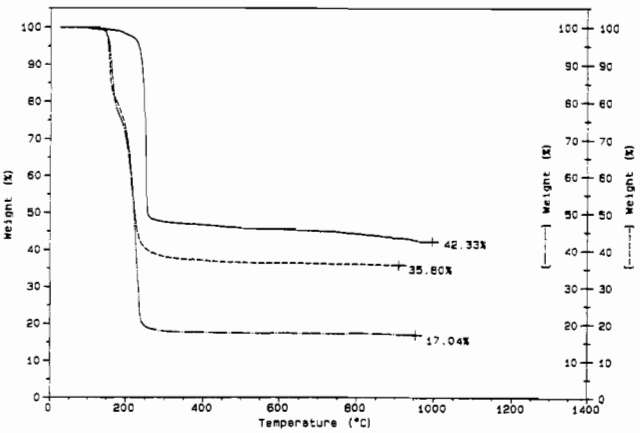

Figure 6. TGA profiles of $Cu_2^{I}Zr_2(O^iPr)_{10}$ (**1**) (dashed–dotted line), $Cu_4^{I}Zr_4O(O^iPr)_{18}$ (**2**) (dashed line), and $Cu_4^{II}Zr_4O_3(O^iPr)_{18}$ (**3**) (solid line). The heating rate is 10 °C/min.

$$\chi_m = \frac{N_g{}^2\beta^2}{3kT}\{[30\exp(-E_Q/kT) + 6\exp(-E_{T_1}/kT) + 6\exp(-E_{T_2}/kT) + 6\exp(-E_{T_3}/kT)]/[5\exp(-E_Q/kT) + 3\exp(-E_{T_1}/kT) + 3\exp(-E_{T_2}/kT) + 3\exp(-E_{T_3}/kT) + \exp(-E_{S_1}/kT) + \exp(-E_{S_2}/kT)]\}$$

The values of the exchange constants found from a least-squares fit of the data were $J_{13} = -60.05$ cm^{-1}, $J_{12} = 34.43$ cm^{-1}, and $J_{14} = 34.39$ cm^{-1} with the g-value fixed at 2.2. This best fit to the data gave an R-factor of 0.051. The relative energies (in cm^{-1}) of the magnetic states are as follows: $E_Q = -8.77$, $E_{T_1} = 128.87$, $E_{T_2} = -60.01$, $E_{T_3} = -60.09$, $E_{S_1} = 197.69$, and $E_{S_2} = -180.15$.

(b) Solution. The magnetic susceptibility was measured in solution using the Evans method[25] with a 2.3 mM solution of **3** in toluene-d_8 with $Si(Me)_4$ as an internal standard. At 294 K and 500 MHz a 8.3-Hz paramagnetic contact shift was observed. Solving for χ_M using eq 4, a value of 1.5×10^{-3} cm^3 mol^{-1} was

$$\chi_m = \left(-\frac{3}{4\pi}\right)\left(\frac{\Delta\nu}{\nu}\right)\left(\frac{10^3\ \text{mL/L}}{C}\right) + \chi_s M - \chi_{dia} \quad (4)$$

obtained. Converting χ_M to μ_{eff} using eq 5 gives a value of 1.9 μ_B/molecule, a value consistent with the solid-state measurements.

$$\mu_{eff} = 2.828\sqrt{\chi_m T} \quad (5)$$

TGA. Thermogravimetric analysis (TGA) studies were conducted on all three copper–zirconium species under a helium atmosphere in order to gain information on their thermal behavior (Figure 6).

Species **1** was found to decompose in a two-step process[26] (eq 6). The first step involves the loss of two isopropoxide ligands

$$\underset{\underline{1}}{Cu_2^{I}Zr_2(O^iPr)_{10}} \xrightarrow[-HOCHMe_2\ -OCMe_2]{140\text{-}160\ ^\circ C} \text{"}Cu_2^{0}Zr_2(O^iPr)_8\text{"} \xrightarrow[-2\ Zr(O^iPr)_4]{160\text{-}325\ ^\circ C} 2\ Cu^0 \quad (6)$$

to acetone and 2-propanol (as detected by mass spectrometry) and the one-electron reduction of each monovalent copper. This is immediately followed by the volatilization of the zirconium isopropoxide moieties, leaving copper metal as the final product by 325 °C.

Compound **2** was also found to decompose in two steps. The first step has an onset temperature of 140 °C and results in a weight loss of approximately 18%. While this value is too large

(25) (a) Evans, D. F. *J. Chem. Soc., Chem. Commun.* **1959**, 2003. (b) Evans, D. F.; Farzakerley, G. V.; Phillips, R. F. *J. Chem. Soc., Sect. A* **1971**, 1931.

(26) For a complete description of the TGA of **1**, see ref 10.

for a $Cu^{I} \rightarrow Cu^{0}$ conversion with loss of $OCMe_2$ and $HO^{i}Pr$ (as in **1**) (theory: 13.7%), the rapid onset of the second decomposition steps produces an inflated weight loss value for the first step. The second step of thermolysis occurs immediately after the first and results in a rapid 46% weight loss. This process is complete by 340 °C, and no further weight loss is observed. XRD revealed the final product to contain copper metal and a significant amount of (metastable) tetragonal zirconia. On the basis of XRD results and the final mass percentage (35.8%), the product contains 4 equiv of copper metal and 3 equiv of ZrO_2. This, in combination with the weight loss profile, allows the decomposition pathway in eq 7to be proposed. While the first step is consistent with the

$$\underset{\underline{2}}{Cu^{I}_{4}Zr_4O(O^{i}Pr)_{18}} \xrightarrow[\text{-2 HOCHMe}_2]{\text{140-160 °C, -2 OCMe}_2} \text{"}Cu^{0}_{4}Zr_4O(O^{i}Pr)_{14}\text{"} \xrightarrow[\text{-5 HO}^{i}\text{Pr}]{\text{160-340 °C, -Zr(O}^{i}\text{Pr)}_4\text{, -5 H}_2\text{C=CHMe}} 4\ Cu^{0} + 3\ ZrO_2 \qquad (7)$$

thermolysis results observed for **1**, the second step appears to be much more complex than that found for the homoleptic heterometallic species. This change of decomposition pathway we attribute to the influence of the oxo ligand. If, after the reduction of the copper, the oxo is able to migrate to the zirconium centers, a transient zirconium oxide–alkoxide species of lower volatility could form, thus preventing the loss of some zirconium fragments (see above). One possibility for such a less volatile molecule is $Zr_3O(O^{i}Pr)_{10}$, a structural type well-precedented in tetravalent metal oxide–alkoxide chemistry.[27] Formation of such a species would leave 1 equiv of zirconium to be lost as the volatile $Zr(O^{i}Pr)_4$. The oxide–alkoxide could then undergo thermolysis producing zirconia and expelling propene and 2-propanol.

Compound **3** was found to decompose via a significantly different pathway. The first step of thermolysis occurs at 180 °C with a small weight loss of 2–3%, corresponding to the release of trace amounts of pentane trapped in the crystalline lattice. This is followed by a rapid 52% loss of weight between 220 and 350 °C. Mass spectral analysis of volatiles indicates the presence of acetone, propene, and isopropyl alcohol. From 350 to 1000 °C, a very gradual (3%) weight loss is observed. Mass spectral analysis of the volatiles show the main product in this temperature range to be water. XRD studies show that the solid products after heating to 600 °C consist of copper metal and zirconia.[28] On the basis of the analytical data, the following thermolysis pathway in eq 8is proposed. It is apparent that, as with compounds

$$\underset{\underline{3}}{Cu^{II}_{4}Zr_4O_3(O^{i}Pr)_{18}} \xrightarrow[\text{-a OCMe}_2\text{, -b H}_2\text{C=CHMe, -c HO}^{i}\text{Pr}]{\text{220 °C-350 °C}} x\ Cu^{0} + y\ ZrO_2 + \text{amorphous material} \xrightarrow[\text{-d H}_2\text{O}]{\text{350 °C-1000 °C}} 4\ Cu^{0} + 4\ ZrO_2 \qquad (8)$$

1 and **2**, internal redox chemistry occurs for the divalent copper species but requires a higher initiation temperature. It is also apparent that no zirconium is lost as volatile species, which is further evidence that the oxo ligands influence decomposition. Species **3** was also decomposed under an atmosphere of dry air. While the decomposition was problematic due to the presence of trace amounts of water affecting the weight loss profile, the thermolysis was found to occur in a single step with an onset temperature of 120 °C. Weight loss was complete by 350 °C. The products were CuO and ZrO_2 (tetragonal and monoclinic).

(27) (a) $Zr_3O(O^{t}Bu)_{10}$: Teff, D. J.; Caulton, K. G. Unpublished results. (b) $U_3O(O^{t}Bu)_{10}$: Cotton, F. A.; Marler, D. O.; Schwotzer, W. *Inorg. Chim. Acta* **1984**, *85*, L31. (c) $Ce_3O(O^{t}Bu)_{10}$: Evans, W. J.; Deming, T. J.; Olofson, J. M.; Ziller, J. W. *Inorg. Chem.* **1989**, *28*, 4027. (d) $Mo_3O(O^{t}Bu)_{10}$: Chisholm, M. H.; Folting, K.; Huffman, J. C.; Kirkpatrick, C. C. *J. Am. Chem. Soc.* **1981**, *103*, 5967.

(28) Diffraction line widths were too broad to distinguish tetragonal from cubic zirconia.

Table 4. VT-XRD Results for Hydrolysis Products

sample	anal. conditions	temp of onset of crystallinity, °C	products
1a	He/TGA residue	N/A	ZrO_2, Cu
1b	He/25–1000 °C	500–700	ZrO_2, Cu_2O
1b	air/25–1000 °C	500–700	ZrO_2, CuO
3a	He/25–1000 °C	approx 500	ZrO_2, Cu_2O
3a	air/25–1000 °C	approx 700	ZrO_2, CuO
"ZrO_2"[a]	air/25–1000 °C	approx 500	ZrO_2

[a] The hydrolysis product of $Zr_2(O^{i}Pr)_8(HO^{i}Pr)_2$ treated as a standard. Preparation identical to sample **1a**.

Hydrolytic Conversion. (a) Hydrolysis. Species **1** and **3** were fully hydrolyzed, and the resulting solids were analyzed via TGA and variable-temperature X-ray diffraction (VT-XRD) under both helium and air. This was to observe the effects of metal oxidation state on thermolysis and the final crystalline product identity. Tetrahydrofuran was chosen as the solvent for hydrolysis due to its miscibility with water and the fact that both heterometallic species are highly soluble and structurally inert in the ether. The alkoxide species were dissolved in THF, and to this was added, with stirring, a THF solution containing an excess of water (7 and 12 mol equiv for **1** and **3**, respectively) over a 2-h period. The resulting reaction mixtures were then allowed to stir for 5 days to ensure complete conversion.

The hydrolysis of **1** resulted in the precipitation of an amber solid from the colorless solution. This solid was isolated via filtration and dried *in vacuo* for 24 h. Removal of solvent from the colorless filtrate produced no residue, indicating that all metal-containing species were contained in the amber precipitate. The dark amber solid was ground up under inert atmosphere producing a light amber powder (**1a**). This powder was found to be free of paramagnetic impurities (as divalent or zerovalent copper) by solid-state magnetic susceptibility measurements but was found to still contain 5.89% carbon and 1.59% hydrogen by elemental analysis. Sample **1a** was very air- (oxygen-) sensitive, rapidly turning a deep green color when exposed. A portion of **1a** was allowed to react with air over a course of 3 days, producing a turquoise powder (**1b**). This powder still contained 1.96% carbon and 1.47% hydrogen by mass. The presence of carbon in the hydrolyzed material indicates the incomplete removal of all the alkoxide ligands, even employing excess water. Such observations have been made before on other metal alkoxides.[29]

The hydrolysis of **3** produced a turquoise precipitate and a colorless solution. Filtration of the reaction mixture produced a green solid which was dried *in vacuo* for 24 h. Removal of solvent from the colorless filtrate produced no residue (see above). The green solid was ground up in air producing a turquoise powder (**3a**). This powder was allowed to stand in air for 3 days with no apparent physical changes. Sample **3a** was found to contain 2.73% carbon and 1.67% hydrogen by combustion elemental analysis.

(b) Thermolysis of the Hydrolysis Products. All hydrolysis products were examined via TGA and VT-XRD in order to observe the effects of thermolysis conditions on the final crystalline products. Results are summarized in Table 4.

The TGA of sample **1a** under helium indicated that the sample underwent numerous unresolved thermolysis steps producing an overall weight loss of 17.1%. XRD of the final product indicated that it consisted of copper metal and the metastable tetragonal phase of ZrO_2. The largest percentage weight loss occurred at low temperatures (100–350 °C), where a 13% change of mass was observed. It is likely that residual organics and trace amounts of water or hydroxyls are lost in this temperature range. From 350 to 1000 °C, the sample continued to gradually lose weight with no distinct steps being resolved.

(29) Brinker, C. J.; Scherer, G. W. *Sol-Gel Science*; Academic Press: San Diego, CA, 1990; Chapter 2.

TGA of **1b** under helium shows a thermolysis profile similar to that of **1a** up to 750 °C. In the lower temperature range (up to 350 °C), 17% weight loss is observed and is followed by a gradual loss of mass (1–2%) up to 750 °C. At this point, a sharp loss of mass (2.2%) was observed, being complete by 825 °C, to leave a final residual mass percentage of 78.9%. The thermolysis of **1b** was also analyzed via VT-XRD to 900 °C under helium. The onset of crystallization occurs above 500 °C (but below 700 °C) with the appearance of CuO and a metastable ZrO_2 phase. In earlier work on the formation of ZrO_2 through low-temperature processing of alkoxides and other monometallic precursors,[30] the material was found by electron microscopy to be nanocrystalline (cubic) rather than truly amorphous. Heating this phase caused the growth of the cubic nanocrystals, followed by a transformation to the tetragonal phase. By 400 °C, the equilibrium monoclinic phase had formed. In our case, the ZrO_2 appears to be predominantly tetragonal or orthorhombic at 700 °C, although the peaks are broad enough that one cannot rule out the presence of some of the cubic phase as well. Upon increase of the temperature to 900 °C, the CuO is transformed to Cu_2O, and the ZrO_2 appears to be a mixture of the metastable tetragonal phase and the equilibrium monoclinic phase. This mixture of phases persists when the sample is cooled back to room temperature.

Thermolysis of **1b** under dry air gave a similar weight loss profile, with a 16.5% drop in weight by 350 °C, but lacked the $CuO \rightarrow Cu_2O$ conversion step at 750 °C, yielding a final mass of 81.2%. This was confirmed by VT-XRD, which showed that initial crystallization of CuO and metastable ZrO_2 occurs at a temperature between 500 and 700 °C. At the latter temperature, the ZrO_2 is predominantly in the cubic phase, with small amounts of the tetragonal phase also present. Upon increase of the temperature to 900 °C, the ZrO_2 transforms completely into the tetragonal phase, which persists, along with the CuO, when the sample is cooled back to room temperature. In this case, we do not see any evidence for the monoclinic ZrO_2 phase.

The thermolysis of **3a** under helium or in air showed that the majority of weight loss occurs by 400 °C. The residual mass at this temperature was significantly different (78.5% and 82.5%, respectively) for TGA studies under helium *vs* dry air. From 400 to 1000 °C, thermolysis under both atmospheres resulted in gradual weight losses to final values of 77.0% for helium and 79.4% for dry air. Using VT-XRD, it was found that heating under helium resulted in the crystallization of Cu_2O at a temperature just below 500 °C, followed by the formation of tetragonal ZrO_2 by 700 °C. In contrast to the thermolysis of **1b** under He, thermolysis of **3a** under these conditions did not produce CuO at any temperature. Under air, crystallization appears only after heating to 700 °C, with CuO appearing initially, followed by ZrO_2 at higher temperatures. In this case, the ZrO_2 lines are wide enough (i.e., particles are small enough) to make distinction between the cubic and tetragonal phases uncertain for any of the temperatures considered.

For all samples studied, no signals in the VT-XRD were observed which could be assigned to a heterometallic oxide phase.

Discussion

Molecular Synthesis and Characteristics. The general advantages of the use of monovalent copper hydrocarbyl species in the synthesis of copper-containing heterometallic alkoxides via deprotonation (eq 9) of coordinated alcohol are 3-fold. First,

$$n\mathrm{CuR'} + \mathrm{M}_l(\mathrm{OR})_m(\mathrm{ROH})_n \rightarrow \mathrm{Cu}_n\mathrm{M}_l(\mathrm{OR})_{m+n} + n\mathrm{R'H} \quad (9)$$

such reactions do not have the inherent complications associated with salt metathesis: halide retention[2a] or the necessity for elevated temperature and/or polar (coordinating) solvents. Second, the use of monovalent copper allows for greater copper-to-heterometal ratios since, purely on the basis of charge balance, two Cu^+ ions can take the place of a cupric ion. For example, the species $Cu_2Zr_2(O^iPr)_{10}$ could be considered as a derivative of $ClCuZr_2(O^iPr)_9$ where the $ClCu^+$ fragment is replaced by a Cu_2OR^+ moiety.[10] Finally, there are numerous precursor species that form stable adducts with acidic protons.[2a,5,31] This allows for a potentially large variety of copper-containing heterometallic species.

Scheme 1

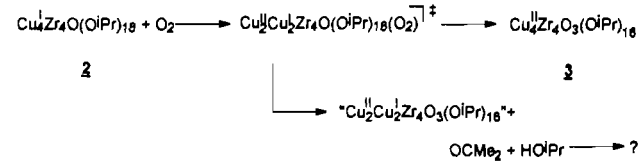

Although cuprous species are vulnerable to oxidative decomposition, this can be an advantage in that Cu^I can be subsequently converted to Cu^{II} with oxygen. In the case of oxidation of copper in **2**, the resulting oxo ligands in **3** bridge the heterometals providing a species which not only is stable to further oxidation[32] but appears to be more resistant to structural degradation by donor solvents.

It has also been shown by the examination of compounds **1–3** that, to a point, one can increase the number of oxo ligands in a precursor without dramatically affecting the solubility of the species. This is due to the fact that O^{2-} is usually found in the interior of the molecular species. Thus, the molecule still has a hydrocarbon exterior. A secondary benefit of oxo ligands is that they can fill numerous metal coordination sites without a dramatic increase in molecular weight (i.e., a μ_4-oxo can replace two μ_2-alkoxide ligands). This may help enhance the volatility of multimetal precursor systems.

Species **3** appears to be a thermodynamic well in copper–zirconium isopropoxide chemistry. The molecule was initially produced from the reaction of 2 equiv of $KZr_2(O^iPr)_9$ with 1 equiv of copper(II) chloride in THF. Since **3** was only produced in low yields and the source of the oxo ligands remained uncertain, other routes to the oxide–alkoxide were investigated. The synthesis of **3** via a combination of salt metathesis and hydrolysis from $K_4Zr_2O(O^iPr)_{10}$, $CuCl_2$ and water was promising in that it produced the copper–zirconium heterometallic in moderate yields. In the course of our investigations of **1**, it was found that **3** was also produced from the reaction of the monovalent copper–zirconium alkoxide with air. While the exact mechanism of formation of **3** from **1** is not known, it is apparent that the reaction occurs in moderate yield. In the case of the conversion of **2** to **3** via O_2, the production of acetone and 2-propanol are the result of an undesired side reaction. This secondary reaction pathway is likely due to the competition of ligand and metal oxidation (i.e., Scheme 1). Given the amount of structural rearrangement required to convert **2** to **3** (conversions of a tetrahedral oxo to square-planar and migration of alkoxides), competing oxidation reactions are not surprising.

(30) Mazdiyasni, K. S.; Lynch, C. T.; Smith, J. S. *J. Am. Ceram. Soc.* **1966**, *49*, 286.

(31) (a) $LiZr_2(O^iPr)_9(HO^iPr)$: Vaartstra, B. A.; Huffman, J. C.; Streib, W. E.; Caulton, K. G. *J. Chem. Soc., Chem. Commun.* **1990**, 1750. (b) $[Ca(hfac)_2(H_2O)_2]_2$: Bradley, D. C.; Hagan, M.; Hursthouse, M. B.; Motevalli, M.; Zhan, O. M. Z.; Pritchard, R. G.; Williams, J. O. *J. Chem. Soc., Chem. Commun.* **1992**, 33. (c) $M_4(\mu_3\text{-}OH)_2(acac)_{10}$ (M = Y, Nd): Hubert-Pfalzgraf, L. G.; Massiani, M. C.; Papiernik, R.; Poncelet, O. *J. Phys.* **1989**, *50*, C5. (d) $[MO^tBu(HO^iBu)]_\infty$ (M = K, Rb): Chisholm, M. H.; Drake, S. R.; Naiini, A. A.; Streib, W. E. *Polyhedron* **1991**, *10*, 337. (e) $Ce_2(O^iPr)_8(HO^iPr)_2$: Vaartstra, B. A.; Huffman, J. C.; Gradeff, P. S.; Hubert-Pfalzgraf, L. G.; Daran, J.-C.; Parraud, S.; Yunlu, K.; Caulton, K. G. *Inorg. Chem.* **1990**, *29*, 3126. (f) Bradley, D. C.; Mehrotra, R. C.; Gacr, D. P. *Metal Alkoxides*; Academic Press: London, 1978; Section 4.13.

(32) In an attempt to gain more information on the oxidation characteristics of species **1–3**, cyclic voltammetry was performed on each compound. No electroactivity was detected from −1.6 to +1.6 V (relative to ferrocene/ferrocenium couple) in dichloromethane.

In this reaction scheme, we propose the formation of a peroxide-containing species as a step in the formation of the divalent copper products. Such ligands are well-precedented in monovalent copper chemistry, particularly in biological systems.[33] It is also thought that peroxo species are intermediates in the copper-catalyzed oxidation of alcohols to ketones. These oxidation reactions appear to go through alkoxide intermediates to produce ketone and water.[30,34] In the chemistry presented here, the oxidation of an isopropoxide ligand would produce acetone and a hydroxyl group, the latter being readily deprotonated by the remaining alkoxide ligands to produce an oxo species and 1 equiv of alcohol.

The structure of **3** exhibits a large number of alkoxide environments, and these are resolvable by ^{1}H NMR. The square-planar oxo ligand is also unusual. For copper systems, no other square-planar oxo systems exist. Square-based pyramidal hydroxide species with all copper centers being coplanar with the central oxygen ligand have been observed for both Cu(I)[35] and Cu(II)[36] species. These systems may be interpreted as square-planar oxo systems where the filled p_z orbital of the oxo has been protonated.[37] Given that the much more common pseudotetrahedral μ_4-oxo (as found in **2**, CuO,[38] and $L_4Cu_4OCl_6$[39]) could satisfy the bonding requirements of the copper centers (as tetrahedral O(5) satisfying both the octahedral zirconium and the square-planar copper), the presence of a square-planar oxo geometry seems to imply other governing causes. Square-planar oxo ligands have been observed previously in both infinite lattice systems (i.e., MO (M = Nb, Ti)[40a-f] and $Sc_{0.75}Zn_{1.25}Mo_4O_7$)[40g] as well as molecular species $[V^{III}_4OCl_8(edt)_2]^{2-}$[23a] and $[Nb^{IV}_4OCl_8\{(PhC)_4\}_2]$.[2-23b] All these systems involve early transition elements and metal–metal bonding. It has been proposed that the square-planar oxo geometry maximizes metal–metal bonding and metal-to-ligand π interactions.[41] In the copper systems, these causes are irrelevant, given the lack of metal–metal bonding and the electron-rich nature of the copper center. While magnetic studies indicate the central square-planar oxo allows for "strong" antiferromagnetic interactions between the unpaired electrons of the trans metal centers (both for the copper and vanadium species), these interactions are too weak to affect ligand geometry. Thus, while there is a basic understanding of the early transition metal–square-planar oxo systems, the reason for the geometry of O(6) in **3** remains an enigma.

Magnetic Characteristics. All attempts to fit the solid-state magnetic data for **3** to a model of lower symmetry (>3 J values) showed no improvement to the fit. The antiferromagnetic character of the exchange coupling, J_{13} = –60.05 cm^{-1}, for the Cu_a–O(6)–$Cu_{a'}$ superexchange can be easily explained. Since the Cu_a–O(6)–$Cu_{a'}$ bond angle is 180° and there is finite overlap of adjacent Cu–O orbitals, then, according to Hund's rule, the interaction of Cu d($x^2 - y^2$)–O p(x,y)–Cu d($x^2 - y^2$) should be antiferromagnetic.[42] Since only two other examples of a planar four-coordinate O^{2-} ion are known,[23] and no magnetic interpretations have been made concerning them, it is impossible to predict the *magnitude* of the antiferromagnetic exchange.

The effect of bridging atom geometry on the sign and magnitude of J in di-μ-hydroxo-bridged Cu(II) dimers as described by Hatfield and Hodgson[43] can be used as the basis for magneto–structural correlations in these and other Cu tetramers. In that work, it was found that there is a linear dependence of the singlet–triplet splitting (2J) on the angle (Φ) at the bridging oxygen. Thus, due to the similarity of the Cu(3)–O(5)–Cu(4) and Cu(3)–O(39)–Cu(4)′ bond angles (94.9 and 94.3°, respectively) and the Cu–O bond distances, the values of J_{12} and J_{14} are nearly equivalent. On the basis of these angles, the positive sign of the exchange coupling constants J_{12} and J_{14} found here is in agreement with the general trend of the 2J *vs* Φ relationship. Since the magnitude of spin–spin coupling in these systems is also a function of the chemical nature of the bridging oxygen atom, we are again unable to predict the *magnitude* of the ferromagnetic J.

The results of a solution magnetic study (Evans method) is in agreement with solid-state results (μ_{eff}(294 K) = 1.1 μ_B/Cu *vs* 0.9 μ_B/Cu, respectively). It is apparent there are no significant magnetic interactions between molecules in the solid state. The similiar values suggest that the solid-state structure is maintained in solution. This conclusion is based on the fact that only perturbation of metal–ligand distances or angles would have a detectable influence on the magnetism of the species, an effect which is not observed.

Thermal Reactivity. It is apparent that the copper centers in these heterometallic alkoxides undergo internal redox with the isopropoxide ligands producing acetone, alcohol and copper metal. This characteristic is independent of metal oxidation state in the precursor molecule or the presence of oxo or halide ligands since **1**–**3** and $ClCu^{II}Zr_2(O^iPr)_9$[10] show similar behavior.

It is interesting to note that the copper alkoxides of **1** have much greater thermal stability as compared to free Cu^IOR. It has been shown that primary (and presumably secondary) monovalent copper alkoxides are unstable at room temperature.[9b] Yet, **1** is stable in solution at 60 °C for days[10] and in the solid state to 140 °C before noticeable decomposition occurs (see Figure 6). This enhanced stability may be due to the electron-withdrawing effect of the zirconium centers, resulting in electron-deficient alkoxides bridging to the copper atom. While this influence of zirconium may explain the stability of the Zr–Cu bridging alkoxides, it does not explain the stability of the Cu_2(O^iPr) ligand. It may be that the presence of more than one electron-rich alkoxide is necessary for the reduction of the copper center.

The divalent copper compounds **3** and $ClCu^{II}Zr_2(O^iPr)_9$ show greater thermal stability (decomposing at 200 and 165 °C, respectively) than the cuprous complexes (decomposing at 140 °C). This enhanced thermal stability reflects the generally greater stability of copper(II) complexes *vs* copper(I) species.[44]

Since the reduction of the cuprous ions to copper metal occurs for all the isopropoxide systems examined, it is apparent that the use of less redox-active alkoxide ligands is desirable if a copper oxide is desired. It has been shown that thermolysis of Cu^IO^tBu initially produces copper oxide (Cu_2O), not copper metal.[9c] Using *tert*-butoxide ligands in heterometallic alkoxide chemistry increases the chances for producing a copper oxide in the final product and potentially enhances the volatility associated with bulky ligands.

It is also apparent that the presence of oxo ligands in the precursor species is beneficial to retention of precursor stoichiometry. In compounds **1**–**3**, each zirconium center has four isopropoxide ligands. Thus, each system could lose the volatile $Zr(O^iPr)_4$ unit and leave behind the copper portion of the molecule.

(33) Karlin, K. D.; Tyeklór, Z.; Zuberbuhler, A. D., *Bioinorganic Catalysis*; Reedijk, J., Ed.; Marcel Dekker, Inc.: New York, 1993; Chapter 4.
(34) Liu, X.; Qiu, A.; Sawyer, D. T. *J. Am. Chem. Soc.* **1993**, *115*, 3239.
(35) McKillop, K. P.; Nelson, S. M.; Nelson, J.; McKee, V. *J. Chem. Soc., Chem. Commun.* **1988**, 387.
(36) McKee, V.; Tandon, S. S. *J. Chem. Soc., Chem. Commun.* **1988**, 385.
(37) For an orbital diagram, see ref 23a.
(38) Asbink, S.; Norby, L.-J. *Acta Crystallogr., Sect. B* **1970**, *26*, 8.
(39) (a) Bertrand, J. A.; Kelley, J. A. *J. Am. Chem. Soc.* **1966**, *88*, 4746. (b) Dickinson, R. C.; Helm, F. T.; Baker, W. A., Jr.; Black, T. D.; Watson, W. H., Jr. *Inorg. Chem.* **1977**, *16*, 1530 and references therein.
(40) (a) Wells, A. F. *Structural Inorganic Chemistry*; 5th ed.; Clarendon: Oxford, U.K., 1984. (b) Braver, G. *Z. Anorg. Allg. Chem.* **1941**, *248*, 1. (c) Anderson, G.; Magneli, A. *Acta Chem. Scand.* **1957**, *11*, 1065. (d) Wantanabe, D.; Terasaki, O.; Jotsons, A.; Castles, J. R. *J. Phys. Soc. Jpn.* **1968**, *25*, 292. (e) Wantanabe, D.; Castles, J. R.; Jotson, A.; Malin, A. S. *Acta Crystallogr.* **1967**, *23*, 307. (f) Hilti, E. *Naturwissenschaften* **1968**, *55*, 130. (g) McCarley, R. E. *Polyhedron* **1986**, *5*, 51.
(41) Burdett, J. K.; Hughbanks, T. *J. Am. Chem. Soc.* **1984**, *106*, 3101.
(42) Hatfield, W. E. In *Theory and Applications of Molecular Paramagnetism*; Boudreaux, E. A., Mulay, L. N., Eds.; Wiley-Interscience: New York, 1976.
(43) Crawford, V. H.; Richardson, H. W.; Wasson, J. R.; Hodgson, D. J.; Hatfield, W. E. *Inorg. Chem.* **1976**, *15*, 2107.
(44) Hathaway, B. J. In *Comprehensive Coordination Chemistry*; Wilkinson, G., Ed.; Pergamon Press: Oxford, U.K., 1987; Sect. 53.1.

In practice, only the systems without oxo ligands lose all the zirconium fragments. $(ClCuZr_2(O^iPr)_9$ also shows a complete loss of zirconium during thermolysis.[10]) With increasing numbers of oxo ligands, there is an increasing amount of zirconium retained in the final product. The oxo ligand helps maintain the metal stoichiometry of the heterometallic precursor during decomposition.

Thermolysis of Hydrolysis Products. Some insight into the scale on which the metal atoms are mixed in the hydrolysis products may be obtained from consideration of the crystallization temperatures we observe. Earlier work on pure ZrO_2 formation from alkoxides found the initial growth of the metastable cubic phase from a nanocrystalline cubic material at temperatures as much as 300 °C below the crystallization temperatures we have found in this study.[30] The presence of copper in our samples may result in a truly amorphous ternary phase (i.e., atomic level mixing) in our processed samples. There is also the possibility that a kinetic phase $Cu_xZr_yO_z$ is present but below the particle size detectable by X-ray diffraction. The barrier to crystallization from this amorphous matrix, and the need for phase segregation of the Cu- and Zr-containing phases, may explain the higher temperatures needed to produce crystals of sufficient size to be seen by X-rays. We also note that the crystallization temperatures we see for the heterometallic species are significantly higher than that seen for the homometallic Zr oxide–alkoxide (see Table 4). Interestingly, we find metastable ZrO_2 phases persisting, in the absence of the monoclinic phase, to well above 700 °C, whereas earlier work[30] saw crystallization of the monoclinic phase at temperatures as low as 400 °C. The higher temperature needed for the formation of the monoclinic phase may reflect the inclusion of small amounts of residual carbon as impurities in our material.

While it is apparent that the hydrolysis of **1** and **3** produced significantly different products (**1a** and **3a**), these hydrolysis products underwent very similar thermolysis. All the samples showed significant weight loss at lower temperatures due to loss of remaining organic contaminants. At higher temperatures, under inert atmospheres, all samples lost oxygen resulting in solids with copper in the next lower oxidation state (i.e., $Cu^{II} \rightarrow Cu^{I}_2$, $Cu^{I}_2 \rightarrow Cu^{0}$). This is not unusual considering the behavior of copper oxide[45] and other mixed-metal copper systems. These materials usually require an external oxygen source to maintain their oxygen content at high temperature. For the hydrolysis products **1b** and **3a**, thermolysis in dry air also showed retention of oxygen. While these samples showed similar thermal characteristics at low temperatures, at high temperature, **1b** was very different from **3a**. VT-XRD and TGA show that thermolysis of **1b** under inert atmosphere produces CuO before converting to Cu_2O. In the case of **3a**, no CuO intermediate is observed and higher temperature is required for crystallinity. On the basis of these results, hydrolysis followed by oxidation (**1b**) does not produce the same products as oxidation in the molecular form (**3a**). It is intriguing to take note of the different crystallization behavior of the solids identified as **3a** and **1b**. These two amorphous solids have similar appearance, and both would appear to contain divalent copper species. Yet upon heating in an He atmosphere, the initial crystallization step for one (**3a**) involves monovalent Cu_2O, while the other, at a different temperature, forms CuO initially. The marked dependence of the crystallization temperature for species **3a** on the atmosphere in which it is contained is also quite remarkable. These differences could indicate two distinct amorphous phases (such as might arise through different short range order in the two solids). Such differences in behavior could also reflect different impurity concentrations or different levels of ligand-induced reduction associated with the distinct routes used to produce what would be the same material under ideal circumstances. Additional studies of the amorphous phase itself will be needed to differentiate these various possibilities; however, it is clear that precursor design can influence the transformation behavior in the solid-state product.

There are no known stable $Cu_xZr_yO_z$ crystalline phases.[46] Although processing techniques such as those used here have the ability to produce metastable crystalline materials, no such metastable heterometallic phases were observed in this study.

Conclusion

This work has shown that oxo complexes of copper–zirconium alkoxides can be produced either by hydrolysis or oxidation with molecular oxygen. These oxide–alkoxide species show significantly different thermal decomposition products as compared to purely alkoxide species (i.e., $M_aM_b'(OR)_n$) in that, with increasing number of O^{2-} ligands, less metal segregation appears to occur. Although the attempts to produce a (currently unknown) mixed-metal oxide via thermolysis or hydrolysis were unsuccessful, results indicated that precursor design did influence the transformation behavior of the solid-state products.

Given the phase separation present during thermolysis, it is possible that precursors could be a route to nanocomposite materials. For the species reported here, the opportunity exists for copper metal, Cu_2O, or CuO crystallites in a zirconia matrix. Such systems may have useful optical, electronic, or catalytic properties. Further efforts are necessary for the synthesis of $Cu_xZr_yO_z$ phases as well as examination of the properties of copper–zirconium oxide nanocomposites.

Acknowledgment. This work was supported by the Department of Energy, as well as a General Electric fellowship (to J.A.S.). We also thank Helmut Rothfuss for technical assistance.

Supplementary Material Available: Tables listing full crystallographic details, anisotropic thermal parameters, and fractional coordinates and *B* values (9 pages). Ordering information is given on any current masthead page.

(45) Cotton, F. A.; Wilkinson, G. *Advanced Inorganic Chemistry*; John Wiley and Sons: New York, 1988; Sect. 18-H-3.

(46) Although $CuZrO_3$ has been reported (Reddy, V. B.; Rao, C. M. R.; Mehrotra, P. N. *Indian J. Chem.* **1981**, *20A*, 81), our analysis of their data indicates the crystalline product is actually a mixture of tetragonal and monoclinic ZrO_2 and CuO.